Disproportionation Channel of the Self-reaction of Hydroxyl Radical, OH + OH → H 2 O + O, Revisited

Xiaokai Zhang, Manuvesh Sangwan, Chao Yan, Pavel Koshlyakov, Evgeni Chesnokov, Yuri Bedjanian, Lev Krasnoperov

Disproportionation Channel of the Self-Reaction of Hydroxyl Radical, $OH + OH \rightarrow H_2O + O$, Revisited

Xiaokai Zhang,[1] Manuvesh Sangwan,[1] Chao Yan,[1] Pavel V. Koshlyakov,[2] Evgeni N. Chesnokov,[2] Yuri Bedjanian,[3] and Lev N. Krasnoperov[1,*]

[1]Department of Chemistry and Environmental Science, New Jersey Institute of Technology, Newark, NJ, 07102. U.S.A.

[2]Institute of Chemical Kinetics and Combustion, Siberian Branch of the Russian Academy of Sciences, Novosibirsk, Russia 630090

[3]Institut de Combustion, Aérothermique, Réactivité et Environnement (ICARE), CNRS, 45071 Orléans Cedex 2, France

Running title: Reaction $OH + OH \rightarrow H_2O + O$

Journal sub-section: Kinetics and Dynamics

[*]Author to whom correspondence should be addressed:
Lev N. Krasnoperov
Department of Chemistry and Environmental Science
New Jersey Institute of Technology, University Heights, Newark, NJ 07102
U.S.A.
FAX: (973)-596-8436
E-mail: lev.n.krasnoperov@njit.edu

Abstract

The rate constant of the disproportionation channel 1a of the self-reaction of hydroxyl radicals OH + OH → H_2O + O (1a) was measured at ambient temperature as well as over an extended temperature range to resolve the discrepancy between the IUPAC recommended value (k_{1a} = 1.48x10^{-12} cm^3 molecule^{-1} s^{-1}, discharge flow system, Bedjanian, Y.; Le Bras, G.; Poulet, G. *J. Phys. Chem.* A **1999,** 103, 7017-7025) and a factor of ca. 1.8 higher value by pulsed laser photolysis (2.7x10^{-12} cm^3 molecule^{-1} s^{-1}, Bahng, M.-K.; Macdonald, R. G. *J. Phys. Chem. A* **2007**, *111,* 3850-3861 and 2.52x10^{-12} cm^3 molecule^{-1} s^{-1}, Altinay, G.; Macdonald, R. G. *J. Phys. Chem. A* **2014**, *118* 38-54).

To resolve this discrepancy, the rate constant of the title reaction was re-measured in three laboratories using two different experimental techniques, laser pulsed photolysis – transient UV absorption and fast discharge flow system coupled with mass-spectrometry. Two different precursors were used to generate OH radicals in the laser pulsed photolysis experiments.

The experiments confirmed the *low* value of the rate constant at ambient temperature (k_{1a}= (1.4 ± 0.2)x10^{-12} cm^3 molecule^{-1} s^{-1} at 295 K) as well as the V-shaped temperature dependence, negative at low temperatures and positive at high temperatures, with a turning point at 427 K:

$$k_{1a} = 8.38\times10^{-14} \times(T/300)^{1.99}\times\exp(855/T) \text{ cm}^3 \text{ molecule}^{-1} \text{ s}^{-1} \qquad (220 - 950\text{K})$$

Recommended expression over the 220 -2384 K temperature range:

$$k_{1a} = 2.68 \times10^{-14} \times(T/300)^{2.75}\times\exp(1165/T) \text{ cm}^3 \text{ molecule}^{-1} \text{ s}^{-1} \qquad (220\text{-}2384\text{K}).$$

Introduction

Hydroxyl radical plays an important role both in the atmospheric[1-7] and in combustion[8-14] chemistry. The self-reaction of hydroxyl radicals is important in the kinetic laboratory studies of other reactions of this intermediate as well as in the fundamental chemical kinetics, as one of the simplest self-reaction of diatomic free radicals:

$$OH + OH \rightarrow H_2O + O \quad (1a)$$

$$\rightarrow H_2O_2 \quad (1b)$$

In the reaction mechanisms reaction 1 contributes as one of the routes of consumption of hydroxyl radicals. In addition, it leads to production of oxygen atoms. In turn, oxygen atoms in subsequent reaction with hydroxyl radicals generate hydrogen atoms, which further complicates data interpretation. Interpretation of the laboratory data requires accurate rate constants and branching ratios with their temperature dependences over a wide temperature and pressure ranges.

Reaction 1 was thoroughly studied both experimentally[15-36] and theoretically.[37-46] A detailed summary of the previous works is given in several publications.[29, 36] The temperature dependence of the disproportionation channel 1a at ambient and slightly elevated temperatures is negative (deceleration of the reaction at higher temperatures), although a positive temperature dependence was reported in one old experimental study.[26] Subsequent experimental studies resulted in a small negative temperature dependence near ambient conditions.[28] Currently, the negative temperature dependence of the disproportionation channel 1a near ambient and slightly elevated temperatures is well established.

However, despite of the large number of experimental studies on the kinetics of reaction 1, the *absolute value* of the rate constant of the disproportionation channel 1a even at the ambient temperature currently is still a subject of a controversy.

The room temperature rate constant of the disproportionation channel 1a, $k_{1a} = 1.48 \times 10^{-12}$ cm^3 $molecule^{-1}$ s^{-1}, as well as the negative temperature dependence at moderate temperatures obtained using discharge flow system[27] are currently accepted in the IUPAC recommendations.[47-48] Later, channel 1a was re-investigated using pulsed photolysis N_2O/H_2O mixtures at 193 nm yielding factor ca. 1.8 higher value of 2.7×10^{-12} cm^3 $molecule^{-1}$ s^{-1}.[29] Kinetics

of reaction 1 was then investigated using photolysis $N_2O/H_2O/O_2$ at 193 nm at high pressures by monitoring ozone formed in the recombination of oxygen atoms produced in channel 1a with molecular oxygen.[36] This study confirmed the lower value of k_{1a} at ambient temperature. In addition, the turning point in the temperature dependence of k_{1a} at ca. 500 K has been reported. In the most recent study, the reaction was re-measured using essentially the same approach as in the previous study of the same group[29] with a modified heatable reactor[49] yielding again a high value of k_{1a} but confirming the turning point in the temperature dependence at ca. 500 K.

In this work, the kinetics of the title reaction was investigated by three research groups using three different techniques to produce hydroxyl radical with two different techniques of monitoring of the decay kinetics. Laser photolysis – time-resolved transient UV absorption of OH at ca. 308 nm were used in the New Jersey Institute of Technology (NJIT) group (Newark, USA) and the Institute of Chemical Kinetics and Combustion (IChK&C) (Novosibirsk, Russia). Two different techniques were used to produce excited $O(^1D)$ atoms: photolysis of N_2O at 193.3 nm (ArF excimer laser, at NJIT) and photolysis of O_3 at 266 nm (4^{th} harmonic of Nd:YAG laser, at IChK&C), respectively. Subsequently, excited oxygen atoms produce OH radicals via fast reaction with water molecules:

$$O(^1D) + H_2O \rightarrow 2\,OH \qquad (2)$$

Fast discharge flow system combined with mass-spectrometric detection was employed in the experiments performed at the *Institut de Combustion, Aérothermique, Réactivité et Environnement,* CNRS, Orléans, France (ICARE/CNRS). In this study, hydroxyl radicals were formed via fast reaction of hydrogen atoms with NO_2:

$$H + NO_2 \rightarrow OH + NO \qquad (3)$$

Hydrogen atoms were produced via microwave discharge in H_2/He mixtures. Hydroxyl radicals were measured via conversion to HOBr in fast reaction of OH with molecular bromine

$$OH + Br_2 \rightarrow HOBr + Br \qquad (4)$$

by subsequent detection of HOBr using mass-spectrometry.

Reaction 1 has two channels, the second (recombination) channel is pressure dependent. This channel was characterized in the previous work over a wide pressure and temperature rangees[36]. Current experiments, devoted to the determination of k_{1a}, were performed at low pressures (1.1 – 7.5 Torr). At these low pressures the contribution of the pressure-dependent channel 1b is small (3 – 10%). This contribution was evaluated based on the results of the previous study over a wide pressure range (1 – 100 bar),[36] and was explicitly taken into account in the reaction model.

All these experiments resulted in a *low* rate constant, $k_{1a}= (1.4 \pm 0.2)x10^{-12}$ cm^3 $molecule^{-1}$ s^{-1} at room temperature. The LCSR/CNRS study performed over an extended temperature range, 220 - 950 K, also resulted in a V-shaped temperature dependence with a turning temperature at 427 K, in excellent agreement with the previous studies of the NJIT group.[36, 50]

Experimental

Pulsed Laser Photolysis – Transient UV Absorption

Pulsed laser photolysis combined with transient UV absorption was used in the studies performed at NJIT (Newark, USA) and IChK&C (Novosibirsk, Russia).

Experimental, NJIT (Newark, NJ, USA)

The details of the experimental set-up and the design of the flow reactor used at NJIT are given in our previous works.[36, 51-53] Hydroxyl radicals were generated in pulsed photolysis of N_2O in the presence of water vapor at 193.3 nm (ArF excimer laser):

N_2O	+	hν (193 nm)	→	$O(^1D)$ +	N_2	(P1a)
			→	$N(^4S)$ + $NO(^2\Pi)$		(P1b)
$O(^1D)$	+	H_2O	→	2OH(v=0,1)		(5a)
			→	$O(^3P)$ +	H_2O	(5b)

$\rightarrow$ H_2 + O_2 (5c)

The quantum yield of the major channel P1a is 100% within the accuracy of 1%, the quantum yield of the minor channel P1b is less than 0.8%.[54]

The fraction of vibrationally excited hydroxyl radicals OH(v=1), formed in the reaction of $O(^1D) + H_2O$ (reaction 5a) is 22-24%.[55-57]

Fraction of $O(^1D)$, formed in photolysis of N_2O, reacts with N_2O:

$O(^1D)$ + N_2O $\rightarrow$ NO + NO (6a)

$\rightarrow$ O_2 + N_2 (6b)

$\rightarrow$ $O(^3P)$ + N_2O (6c)

The hydroxyl radical temporal profiles were recorded via multiline UV absorption at ca. 308 nm using low pressure H_2O/Ar DC discharge lamp.[36]

To provide uniformity across the cross-section of the reactor, before entering, the photolysis laser beam was formed with two lenses: a spherical, with the focal length of 30 cm, located 70 cm from the reactor entrance, and a cylindrical, with the focal length of 30 cm, located 23 cm from the reactor. This arrangement provided the beam uniformity across the reactor's cross-section of ± 7.3% from the mean value.

The bath gas used in all experiments was helium. The measurements were performed at ambient temperature at pressures of 0.01, 0.1 and 1 bar. The path length of the reaction zone was precisely defined using the 4-window configuration of the reactor.[36] Brooks mass flow controllers (model 5850) were used to control the bath gas and the reactants flow rates. The total flow rates were in the range 20 – 75 sccs. Flush flows to the reactor windows were in the range 4.5 - 10 sccs. Precision syringe pump (Harvard Apparatus, Model PHD 4400) was used to inject liquid water through a capillary tube into an evaporator (kept at 90 ^oC) and, subsequently, to the reactor. The flowrate of liquid H_2O was in the range 6 – 18 μl/min.

In Situ Actinometry. The absolute concentrations of OH radicals were determined based on the photon flux inside the reactor, the absorption cross-section of N_2O at 193.3 nm, and the effectiveness of conversion of $O(^1D)$ atoms, produced in the photolysis of N_2O, to OH radicals. The conversion of $O(^1D)$ to OH was about 0.84x2 as accurately evaluated using a reaction

mechanism. The absorption cross-section of N_2O is known at 298 and 1 bar with good accuracy,[58] at other conditions the cross-sections of N_2O were measured in the previous works.[36] To avoid the errors associated with the determination of the laser light intensity inside the reactor using outside energy meters (which require independent calibrations) as well as the windows transmittance drift due to film deposition caused by contaminations, *in situ* laser light actinometry was used. The approach is based on the monitoring of ozone formation at 253.6 nm in the photolysis of $N_2O/O_2/N_2$ mixtures at 1 bar and 298 K.[36]

The details of such measurements are described elsewhere.[35-36, 59-60] Briefly, N_2O, diluted with 5.0% O_2 in N_2 mixture was pumped through the reactor at ambient (measured) pressure and photolyzed at 193.3 nm. Temporal profiles of O_3 build-up were monitored using a low pressure RF discharge mercury lamp at 253.7 nm. After formation in the photolysis, excited oxygen atoms $O(^1D)$ undergo relaxation in collisions with nitrogen ($k_{q,N2} = 2.6x10^{-11}$)[61] and oxygen ($k_{q,O2} = 4.0x10^{-11}$)[61] or react with N_2O ($k = 1.35x10^{-10}$). The concentration of oxygen-nitrogen mixture ($2.43x10^{19}$ molecule cm^{-3}) used in these experiments was much higher than the concentration of N_2O ($7.4x10^{16}$ molecule cm^{-3}) which provided almost complete (98.5%) relaxation of $O(^1D)$ to the ground state oxygen atoms $O(^3P)$ and subsequently to conversion to ozone in fast reaction with molecular oxygen, $O(^3P) + O_2 + M \rightarrow O_3 + M$. The absorption cross-section of N_2O at 193.3 nm used in these determinations is the JPL recommended value, $\sigma_{N2O} = 8.7x10^{-20}$ $cm^2molecule^{-1}$ (at 298 K and 1 bar).[62] The technique is described in detail in Ref.[36]

The uncertainty in the measured rate constant is estimated based on the uncertainty in the absolute concentrations of hydroxyl radicals, uncertainty associated with the reaction model, and the statistical error in the decay parameters. The accuracy of the N_2O cross-sections (ca. ±6%), the O_3 determination (ca. ±4%), and the uncertainties introduced by the ozone formation model (ca. ±3%) contribute to the accuracy of the determination of the absolute concentrations of OH radicals. The uncertainties associated with the reaction model are estimated as ±11%. The statistical errors in the decay parameters of OH radicals at low pressures used in this work are negligible. Assuming that all these sources are independent, the overall estimate of the accuracy of the rate constants is ±14% (±2σ).

In the experiments, two determinations of the photon flux inside the reactor were performed, before and after a series of measurements. In every accumulation of a kinetic profile the readout of the pyroelectric detector installed after the reactor was recorded. This readout was

used then to introduce proper corrections for the drift of the laser energy during the series of experiments.

Subsequently, the apparent absorption cross-section of OH radical on the multi-line radiation near 308 nm determined using the *in situ* actinometry was used to calculate the absolute concentrations of OH in the kinetic measurements. Detailed results on the temperature and pressure dependence of the absorption cross-section of OH are given in a previous publication.[36] At ambient temperature (295 ± 3) K and low pressures (< 0.1 bar) the cross-section is 5.02×10^{-17} $cm^2 molecule^{-1}$.

The concentrations of the precursors used were $(4.6 - 6.4) \times 10^{16}$ molecule cm^{-3} (N_2O), $(3.7 - 11.0) \times 10^{17}$ (H_2O) and $(3.9 - 5.5) \times 10^{17}$ (O_2). The photolysis laser photon fluence inside the reactor was varied in the range $(4.6 - 8.9) \times 10^{15}$ photon cm^{-2} $pulse^{-1}$. The initial concentrations of hydroxyl radicals were in the range $(4.7 - 8.4) \times 10^{13}$ molecule cm^{-3}. The pressure range of the current study was 0.01 – 1 bar (He). The experiments were performed at ambient temperature of 293 ± 3 K. The repetition rate of the laser was adequate to ensure complete replacement of the gas mixture in the reactor between the pulses (0.3 – 2 Hz, depending on pressure).

As it was observed in numerous experiments, the lifetime of hydroxyl radical in uncoated reactors (quartz, stainless steel) was too short (< 0.5 ms) due to wall decay, which prevented any kinetic measurements unless a wall coating was used. In the initial experiments, Halocarbon Wax was used to reduce the wall activity to an acceptable level. However, this material absorbs 193 nm light, so that the windows of the reactor could not be coated. Fast decay of OH on the reactor windows leads to short transients in the OH kinetic curves due to the establishing of a diffusion-against-flow concentration profile near the windows. This annoying transient complicated the data interpretation.

At a later stage, a new wall coating witch works superior to Halocarbon Wax was found. This is perfluoropolyether, $F\text{-}(CF(CF_3)\text{-}CF_2\text{-}O)_n\text{-}CF_2\text{-}CF_3$, which is commercially available as synthetic vacuum oil under several different brand names. Specifically, we used DuPont Krytox 1525. This polymer is chemically inert and transparent in the UV and far-UV, including 193 nm. Therefore, it could be used to coat the windows both at 266 nm and 193 nm over an extended temperature range. It has very low vapor pressure (1×10^{-7} Torr at 20 ^oC and 2×10^{-3} Torr at 200 ^oC). In a reactor with ID of 0.7 cm, observed wall decay rate constant for hydroxyl radicals is

about $k_{w,OH}$ = 15 – 28 s^{-1} (lifetime of 36 – 70 ms), which results in the probability of decay per collision of $\gamma_w(OH) = (1.7 – 3.2) \times 10^{-4}$.

Reagents. Helium used in the experiments was BIP®Helium from Airgas with 99.9999% purity and with reduced oxygen content (<10 ppb). UHP oxygen was obtained from Matheson TriGas (99.98% purity). Certified mixture of N_2O in He (2.50%, accuracy ±2%) obtained from Matheson Tri-Gas was used. Purified water (Milli-Q®) with TOC less than 5 ppb) was degassed by freeze-pump-thaw cycles and used as a reactant supplied by a syringe pump (Harvard Apparatus PHD 4400) as well as in the low pressure H_2O/Ar discharge hydroxyl monitoring lamp. UHP Argon obtained from Matheson TriGas (99.999% purity) was used in the H_2O/Ar lamp.

Experimental, IChK&C (Novosibirsk, Russia)

The only essential difference of the experimental approach used at IChK&C was in the photochemical generation of excited oxygen atom via photolysis of ozone at 266 nm using the 4th harmonic of Nd-YAG laser (Lotis Tii, model: LS-2137U, the energy in the 4th harmonic of 130 mJ at the pump lamp energy of 36 J)

$$O_3 + h\nu\ (266\ nm) \rightarrow O_2 + O(^1D) \qquad (P2)$$

The optical arrangement was similar, but not identical to the arrangement used at NJIT. A low pressure Hg lamp was used to measure the ozone kinetics for the purpose of the *in situ* actinometry, DC discharge low pressure OH-lamp identical to the one at NJIT was used to measure the absorption of OH radical near 308 nm. A prism monochromator (Carl Zeiss, SPM2) was used in these studies. Before entering the reactor, the laser beam was formed by a diaphragm with a diameter of 6.44 mm. The root-mean-square inhomogeneity of the laser beam was ± 12% from the mean value. The apparent cross-section of hydroxyl radicals in the set-up at IChK&C determined from the *in situ* actinometry measurements differ from the one obtained at NJIT, even though an identical design as well as the electrical parameters of the DC discharge in H_2O/Ar lamp were used. This difference was assigned as being due to the somewhat different optical arrangements of the lenses that formed the monitoring beam. The apparent cross-section

depends upon the gas temperature in the discharge, which has a radial distribution. Thus, the regions closer to the discharge tube axis would emit light which would be absorbed less efficiently compared to the light emitted from the regions closer to the discharge tube wall. Finally, the resulting apparent cross-section depends upon the relative contributions of the light emitted in different places of the discharge tube, which, in turn, depends on the beam forming lenses positions, focal distances, as well as the monochromator slits widths. The apparent cross-section of OH at ambient temperature (295 K) and low pressures (< 0.1 bar) measured using the set-up at IChK&C, was 7.2×10^{-17} cm^2 $molecule^{-1}$.

Helium was used as the bath gas in all measurements. The measurements were performed at ambient temperature at pressures 0.01 and 0.02 bar. Gas flow rates were controlled by mass flow controllers (Tylan, model FC 260). The total flow rates of the reactant mixtures with helium were in the range 0.75-0.83 sccs. Water vapor was supplied via a two-stage impinger with controlled temperature.

In Situ Actinometry. The absolute concentrations of OH radicals were determined based on the photon flux inside the reactor, the absorption cross-section of O_3 at 266 nm, and the efficiency of conversion of $O(^1D)$ atoms produced in the photolysis of O_3 to OH radicals. The latter was typically about 0.97 and was accurately evaluated using a reaction mechanism. The absorption cross-section of O_3 is accurately known at 298 and 1 bar.[58] Again, an *in situ* laser light actinometry was used. In this case ozone depletion was monitored at 253.6 nm in the photolysis of $O_3/O_2/N_2$ mixtures at 0.02 bar and 298 K. This is the same technique that was used to determine *in situ* photon flux via ozone *depletion* in photolysis at 248 nm.[63] Sample ozone absorption trace used in the *in situ* actinometry as well in the additional measurements of k_{1a} are shown in the Supporting Information (Fig. S1).

In the experiments, ozone was formed on line using dielectric barrier discharge ozonator (50 Hz, up to 11.3 kV) in O_2/He mixtures. The home-made ozonator was a dielectric barrier discharge tube with a grounded electrode outside of the tube (aluminum foil) and a thin Ni-Cr coaxial wire inside the reactor as the high-voltage electrode. The ozonator power and, subsequently, the ozone yield, was controlled by variation of the input voltage of the high voltage transformer. The maximum conversion of oxygen to ozone in the experimental conditions used was 7 %. The concentration of ozone in the reactor was measured via the absorption at 253.6 nm.

The walls of the reactor, as well as the windows in some experiments, were coated with either Halocarbon Wax or Krytox 1525, as described in the previous section.

The concentrations of the precursors used were $3x10^{13} – 2x10^{15}$ molecule cm^{-3} (O_3), $(1.5 – 6.8)x10^{16}$ (H_2O) and $2.8x10^{15} – 4x10^{17}$ (O_2). The photolysis laser photon fluence inside the reactor was varied in the range $6.3x10^{14} – 9.7x10^{15}$ photons $cm^{-2}pulse^{-1}$. The initial concentrations of hydroxyl radicals were in the range $1x10^{13} – 1.3x10^{14}$ molecule cm^{-3}. The experiments were performed at ambient temperature 293 ± 3 K and low pressures in the range 0.01-0.02 bar. The repetition rate of the laser was adequate to ensure complete replacement of the gas mixture in the reactor between the pulses (5.7 Hz).

Reagents. Helium used in the experiments was 99.995% purity with reduced oxygen content (10^{-4}%). UHP oxygen used has purity of 99.95% Deionized water with electrical resistivity of 17 MOhm*cm was used. UHP Argon (99.999%) was used in the H_2O/Ar discharge lamp.

Fast Discharge Flow – Mass-Spectrometry

Experimental – ICARE/CNRS (Orleans, France)

The title reaction was studied with a discharge flow reactor at total pressure of helium of 1 – 2 Torr using a modulated molecular beam mass spectrometer as the detection method.[27, 64-65] Two flow reactors were used. The first one, used at low temperatures (220 – 318 K), consists of a Pyrex tube (45 cm length and 2.4 cm i.d.) with a jacket for the thermostated liquid circulation (ethanol). The walls of the reactor as well as of the movable injector of OH radicals were coated with halocarbon wax in order to minimize the heterogeneous loss of OH. The second flow reactor used at high temperatures (T = 295 – 950 K), consisted of an electrically heated Quartz tube (45 cm length and 2.5 cm i.d.) with water-cooled attachments (Supporting Information, Fig. S2).[64] In contrast to the pulsed experiments at NJIT and IChK&C, *no surface coatings* of the quartz tube and the injector were used in the experiments at elevated temperatures. Temperature in the reactor was measured with a K-type thermocouple positioned in the middle of the reactor in contact with its outer surface. Temperature gradient along the flow tube (Supporting

Information, Fig. S2) measured with a thermocouple inserted in the reactor through the movable injector was found to be less than 1%.[64]

Hydroxyl radicals were produced in the main reactor through a rapid reaction of H atoms with excess NO_2, hydrogen atoms being generated in a microwave discharge of H_2/He mixtures (Supporting Information, Fig. S2):

$$H + NO_2 \rightarrow OH + NO \quad (3)$$

$k_3 = (1.47 \pm 0.26) \times 10^{-10}$ cm^3 molecule^{-1} s^{-1} (T = 195 – 2000).[66]

Hydroxyl radicals were detected at m/z = 96/98 ($HOBr^+$) after being scavenged with an excess of Br_2 (added in the end of the reactor 5 cm upstream of the sampling cone, as shown in Supporting Information, Fig. S2 through reaction 4:

$$OH + Br_2 \rightarrow HOBr + Br \quad (4)$$

$k_4 = 2.16\times10^{-11} \exp(207/T)$ cm^3 molecule^{-1} s^{-1} (T = 220 - 950K). [67]

Reaction 4 was also used for the determination of the absolute concentrations of OH. In excess of molecular bromine, the consumed fraction of Br_2 is equal to the concentration of HOBr produced, which, in turn, is equal to the concentration of hydroxyl radicals: [OH] = [HOBr] = $\Delta[Br_2]$. The possible influence of secondary chemistry on this method of the detection of OH radicals and their absolute calibration procedure was discussed in details in the previous studies from this group.[27, 65] The concentrations of stable species (NO_2 and Br_2) were calculated from their flow rates, which were measured using pressure drops of their mixtures in He stored in calibrated volume flasks.

Reagents. The purities of the gases used were as follows: He (>99.9995%, Alphagaz), passed through liquid nitrogen trap; H_2 (> 99.998%, Alphagaz); Br_2 (>99.99%, Aldrich); NO_2 (> 99%, Alphagaz).

Results

Photolysis of $N_2O/H_2O/He$ mixtures at 193.3 nm (NJIT)

Sample OH decay absorption profiles of OH radicals at different initial concentrations are shown in Fig. 1. Since the wall decay rate constant is initially unknown, the following iterative approach was used to process the experimental data. First, the "initial slope rate constant", k', was determined using exponential fitting through the initial part of the decay curve. Typically, the initial part of the decay curve that corresponds to ca. 33% of the amplitude decay was used. Then, the resulting k' was plotted vs. the absorption amplitude as to yield a straight line with an intercept. (Fig. 2) The intercept is due to the wash-out of the gas mixture from the reactor (a well-defined contribution) and the rate constant of the wall decay of hydroxyl radicals, $k_{w,OH}$. The intercept was used then to determine the first approximation to the hydroxyl radical wall decay rate constant, $k_{w,OH}$ The slope could be also used to determine the first approximation to the rate constant of the channel 1a using the apparent stoichiometric coefficient calculated via modeling with the complete reaction mechanism. The complete reaction mechanism for the $N_2O/H_2O/He$ + 193 nm photolysis system is described in detail in our previous publications.[35-36, 50] For reference, the mechanism which was used for the data processing is also given in the Supporting Information, Table S1.

Then the original absorption profiles were fitted using the full kinetic model by numerical solution of the ODE system corresponding to the reaction mechanism using SCIENTIST software.[68] The first approximation wall rate constant obtained via the "initial slope" analysis is used in the reaction model. The wash-out contribution is explicitly and correctly installed in the fitting model. The resulting product $k_{1a}[OH]_{ini}$ is plotted vs. the $[OH]_{ini}$, the resulting intercept is used to adjust the wall decay rate constant, $k_{w,OH}$, until the intercept becomes zero. In this specific example, the procedure converged in two additional steps beyond the initial slope analysis, yielding the rate constant k_{1a} of 1.39×10^{-12} cm^3 $molecule^{-1}$ s^{-1} with the wall loss rate constant for hydroxyl radicals of $k_{w,OH} = 28$ s^{-1}. It should be stressed, that although all relevant reactions have been included in the mechanism, only four reactions are sufficient to account for 93% of the returned rate constant k_{1a}, namely the two channels of reaction 1, reaction of oxygen

atoms with OH and the wall reaction of hydroxyl radicals. Inclusion of all other processes in the reaction mechanism leads to a correction that does not exceed 7% of the rate constant.

Photolysis of $O_3/O_2/H_2O$/He mixtures at 266 nm (IChK&C)

Sample kinetic profiles of OH absorption in the photolysis of $O_3/O_2/H_2O$/He mixtures using the 4th harmonic of a Nd:YAG laser (266 nm) are shown in the Supporting Information, Fig. S3. The corresponding plot that results from the processing of these data is shown in Fig. 4. In this series of measurements, the reactor walls as well as the internal surfaces of the fused silica windows were coated with Halocarbon Wax. The plot in Fig. 4 shows the last iteration of the iteration procedure as described in the previous section. The presence of molecular oxygen in the reaction mixture is due to the incomplete conversion to ozone in the inline dielectric barrier discharge ozonator. The wall decay rate constant, $k_{w,OH}$ = 15 s^{-1}, the returned rate constant k_{1a} = (1.34 ± 0.10)x10^{-12} cm^3 molecule^{-1} s^{-1} (± 3 σ). In the photolysis of ozone containing mixtures, the kinetic information on the rate constant k_{1a} can be obtained based on the OH decay profiles as well as on the O_3 decay profiles. Ozone has a very large absorption cross-section at 266 nm, and only small amounts of ozone are required to produce the desirable concentrations of OH radicals. Therefore, the depletion of ozone in the reaction with OH is not negligible, and can be used for the determination of the rate constant k_{1a}. In Fig. 4, the circles are obtained by processing of OH absorption profiles (at ca. 308 nm), while the squares are obtained by processing of O_3 absorption profiles (at 253 nm, Hg lamp). Both determinations are in excellent agreement, as shown in Fig. 4.

Fast Discharge Flow – Mass-Spectrometry Experiments ICARE/CNRS (Orleans, France)

The rate constant of the title reaction 1a was determined from the kinetics of OH consumption in the temperature range 220-950 K and 1.0-2.2 Torr total pressure of He. Temporal profiles of OH were monitored for different initial concentrations of the radicals in the presence of relatively high concentrations of NO_2 in the reactor ((2-5)×10^{13} molecules cm^{-3} (from the OH source). Typical examples of the experimental profiles obtained at two extreme temperatures of the study (T = 220 and 950 K) at different initial concentrations of OH radicals

are shown in Fig. 5. Partially shown error bars represent maximum uncertainty of 5% of the measurements of the relative concentrations of OH. Some other examples of the kinetic runs are shown in Supporting Information, Figs. S4, S5. The experimental data were processed using a simple kinetic mechanism of reactions 1a and 7:

$$OH + OH \rightarrow O + H_2O \quad (1a)$$

$$OH \rightarrow loss \quad (7)$$

Reaction 7 is a lump sum of several processes: the heterogeneous loss of OH radicals on the wall of the flow reactor ($k_{w,OH}$), the reaction of OH with NO_2, and the possible secondary reaction between OH and HNO_3:

$$OH + wall \rightarrow loss \quad (8)$$

$$OH + NO_2\ (+M) \rightarrow HNO_3\ (+M) \quad (9)$$

$$OH + HNO_3\ (+M) \rightarrow H_2O + NO_3\ (+M) \quad (10)$$

In contrast to the time-resolved pulsed photolysis experiments discussed above, the secondary reactions initiated by the oxygen atoms formed in reaction 1a in these experiments do not play role in the OH kinetics due to the presence of NO_2 (see below).

In the frames of the simple two step mechanism (reactions 1 and 7), the rate of OH consumption is:

$$d[OH]/dt = -2k_1[OH]^2 - k_7[OH] \quad (E1)$$

An analytical solution of this differential equation leads to the following expression for the temporal profiles of OH radicals:

$$[OH] = k_7[OH]_0/[(2k_{1a}[OH]_0 + k_7)\times\exp(k_7t) - 2k_{1a}[OH]_0] \quad (E2)$$

The measurements were performed over a wide range of the initial concentrations of OH radicals to reliably decouple the rate constant of interest, k_{1a}, and the pseudo-first order rate constant k_7 (Fig. 5). At low initial concentrations, the second order reaction 1a is almost negligible, and the decay temporal profiles are exponential (linear dependences in the log scale of Fig. 5). These measurements provide reliable determination of k_7. At high initial concentrations, strong deviations from exponential decay are apparent (strongly curved plots in the log scale, Fig. 5). These temporal profiles with high initial concentrations of OH radicals provide reliable determination of the bimolecular rate constant k_{1a}. At each temperature, the rate constant of reaction (1a) was derived from the *global fit* to all experimental kinetic runs using equation E2 with two variable parameters, k_{1a} and k_7. The results of the fits are shown in Fig. 5 as solid lines. The ranges of the initial concentrations of OH radicals used and the results obtained for k_1 and k_7 at different temperatures are shown in Table 1.

The possible impact of the secondary reactions on the results of the measurements of k_{1a} was discussed in the previous study from the Orléans group,[27] where a similar experimental approach and similar experimental conditions were used. Briefly, the secondary chemistry initiated by the O-atoms formed in reaction 1a,

$$O + NO_2 \rightarrow NO + O_2 \qquad (11)$$

$k_{11} = 9.85\times10^{-16} T^{1.41} \exp(543/T)$ cm^3 molecule^{-1} s^{-1} (T = 220 – 950 K)[69]

$$O + OH \rightarrow H + O_2 \qquad (12)$$

$k_{12} = 1.8\times10^{-11} \exp(180/T)$ cm^3 molecule^{-1} s^{-1} (T = 136 – 515 K),[62]

has no impact on the kinetics of OH consumption, because hydrogen atoms formed in reaction 12 are rapidly converted back to OH in reaction with NO_2.

In the determination of k_{1a}, the rate of the lump-sum reaction 7, $k_7 = k_{w,OH} + k_9[NO_2]+k_{10}[HNO_3]$, was considered as independent of the initial concentration of OH, that is constant for all the kinetic runs at each temperature. This assumption seems to be reasonable,

despite the negative and positive concentration gradient along the reaction zone for NO_2 and HNO_3, respectively. First, the mean concentration of NO_2 along the reaction zone ((3.5-4.5)×10^{13} molecules cm^{-3}) was kept constant for all the kinetic runs of OH, at a given temperature. Second, numerical simulations performed in a previous study from the Orléans' group (under similar experimental conditions), showed that even at the lowest temperature of that study (T = 233 K) that is, for the maximum values of the rate constants of reactions 9 and 10, the contribution of reaction 10 to OH loss rate was negligible (<5%) compared to the contribution due to the heterogeneous loss and reaction 9.[27] The rate constants for the reactions 9 and 10 used in those calculations, $k_9 = 2.5\times10^{-30}$ $(T/300)^{-4.4}$ $cm^6 molecule^{-2} s^{-1}$ (for M = N_2) and $k_{10} = 2.1\times10^{-13}$ cm^3 $molecule^{-1} s^{-1}$ (T = 230 K), are supported by recent measurements. The rate constant of reaction (10) depends on pressure and identity of the bath gas.[70] Recently, the measurements of k_{10} at T = 217 - 695 K and p = 0.56 – 8.24 Torr with He as a third body have been reported.[71] The temperature dependence of the rate constant was found to be V-shaped with a value of k_{10} = 2.1×10^{-13} cm^3 $molecule^{-1} s^{-1}$ at T = 220K, the lowest temperature of the present study.[71] For the reaction OH+NO_2 (+M), recently reported value of $k_9 = 2.0\times10^{-30}$ $(T/300)^{-3.6}$ $cm^6 molecule^{-2} s^{-1}$ (for M = O_2)[72] is even lower than that used in the simulations and, in addition, should be considered as an upper limit under our experimental conditions. This is due to two factors. First, the collision efficiency of He (the bath gas in the present study) is lower than the collision efficiency of O_2. Second, there is an evidence that reaction 9 is in the pressure fall-off region at pressures of ca. 2 Torr.[72] Finally, in order to verify a possible impact of the reactions 9 and 10 on the measurements of k_{1a}, we have conducted three series of experiments at the lowest temperature of this study (T = 220 K) with different concentrations of NO_2 and at total pressures of 1.1 and 2.2 Torr. The measurements at 1.1 Torr, carried out with [NO_2] = 2x10^{13} and 5×10^{13} molecule cm^{-3}, resulted in k_7 increasing from 10.4 to 18.0 s^{-1}, and practically identical k_{1a} = 2.07 and 2.13×10^{-12} cm^3 $molecule^{-1}$ s^{-1}, respectively. Similar value of $k_{1a} = 2.10\times10^{-12}$ cm^3 $molecule^{-1}$ s^{-1} was derived from the measurements at 2.2 Torr with [NO_2] = 2×10^{13} molecule cm^{-3}. These observations, as well as the consistency of the results obtained at all temperatures for k_1 and k_7 with a widely varied initial concentrations of OH, suggest that all processes that impact the loss of OH are properly taken into account.

In fact, under the experimental conditions where initial concentration of OH is largely varied, the two variables in equation E2, k_{1a} and k_7, can be determined practically independently

of each other. At the lowest concentrations of OH, the OH loss kinetics is not sensitive to k_{1a}, while at highest $[OH]_0$, the kinetics of OH is driven mainly by consumption of the radicals in reaction 1a. This is demonstrated in Figure S5 (SI): one can see that the variation of k_1 within 10% leads to a significant deviation of the calculated OH profiles (dashed lines) from the experimental data points at the highest $[OH]_0$ with a negligible impact at the lowest initial concentration of OH. We estimate statistical uncertainty of ≤ 10% in the determination of k_{1a} through the fit to the experimental data with equation E2. The total combined uncertainty of the measurements of k_{1a} is estimated to be of about 15%, by adding in quadrature (square root of the sum of squares), the statistical error (≤ 10%), and those of the measurements of the flow rates (5%), pressure (2%), temperature (1%), and absolute concentrations (≤ 10%) of OH radicals.

The experimental conditions as well as the resulting rate constants k_{1a} are summarized in Table 1.

The results of the current study together with the results of previous recent studies are shown in Figure 6. The data were fitted using the Modified Arrhenius Expression (three parameters, A, n and E). The results are:

Fit to the data from the present work (blue line):

$$k_{1a} = 8.38\times10^{-14} \times(T/300)^{1.99}\times\exp(855/T)\ \text{cm}^3\ \text{molecule}^{-1}\ \text{s}^{-1}\ (T = 220\text{-}950\text{K}) \qquad \text{(E3)}$$

Fit to all data (except Ref. [49] [29], black line):

$$k_{1a} = 2.68\times10^{-14} \times(T/300)^{2.75}\times\exp(1165/T)\ \text{cm}^3\ \text{molecule}^{-1}\ \text{s}^{-1}\ (220\text{-}2384\text{K}). \qquad \text{(E4)}$$

The two expressions E3 and E4 result in almost identical values for the turning temperature of the V-shaped temperature dependence, 427 and 423 K, respectively. The dashed lines correspond to the ± 20% deviation from the expression E4 (Fig. 6, black line), showing that almost all experimental points fall within these limits.

Discussion

Reaction 1 has two channels, the recombination channel 1b is pressure dependent. The contribution of pressure dependent channel 1b at 298 K and 0.01 bar is 1.55×10^{-13} cm^3 $molecule^{-1}$ s^{-1}, which is ca. 10% of the total rate constant at these conditions. The contributions at higher temperatures are smaller. In the discharge flow – MS experiments performed at 1.1 – 2.2 Torr this contribution does not exceed 3%. In the laser photolysis – transient absorption experiments this (small) contribution was accurately calculated based on the factorization from Ref. [36] and explicitly included in the reaction model.

The three experimental studies using two different approaches and three different techniques to generate OH radicals unambiguously confirmed the *lower* value of the rate constant of the disproportionation channel 1a. The discrepancy between the current as well as several previous studies with the most recent studies of the Argonne group[29, 49] requires some discussion. Although the photolysis system used to generate OH radicals used in[29, 49] (N_2O/H_2O/He photolysis at 193.3 nm) is the same as the one used by the NJIT group in this work, there are several differences in the reaction conditions as well as the design of the reaction cell. The measurements in[29, 49] were performed with the mixtures with relatively high $[N_2O]/[H_2O]$ ratios (0.5 – 6), compared with the current NJIT study (ca 0.1). The second important difference in the cell design and the experiment arrangement. In the NJIT as well as IChK&C studies, the reaction was a cylindrical tubing, so that the reaction was limited in space by the reactor walls, coated with inert coatings. The homogeneous distribution of the free radicals over the cross-section of the reactor is provided by the beam forming to achieve homogeneous light intensity over the cross-section of the reactor as well as by fast radial diffusion (<0.5 ms), on the timescale which is much shorter than the typical reaction times (3 – 30 ms). In both studies of the Argonne group, the reaction zone is initially determined by the geometry of the photolysis light, with subsequent losses by free diffusion out of the photolysis and the observation zone.

The main concern associated with the high $[N_2O]/[H_2O]$ ratios is in the possible participation of "hot" hydroxyl radicals formed in the reaction of excited oxygen atoms with water molecules:

$$O(^1D) + H_2O \rightarrow OH^{**} + OH^{*} \qquad (2a)$$

As it was already stated, significant amounts of hydroxyl radicals formed in this reaction are vibrationally excited, v=1,2. Moreover, the two hydroxyl radicals formed have very high rotational temperatures, ca. 2600 and 6000 K,[57, 73] respectively. Due to the large rotational constant of OH radical, one can assume that the rotational relaxation of high J levels in collisions with helium atoms is not fast. Then, the ratio of the concentrations of N_2O and H_2O might play a role. At high concentrations of H_2O the relaxation on water molecules of both vibrationally and rotationally excited OH radicals would be much faster than a possible reaction of hot OH radicals with N_2O:

$$OH^* + N_2O \rightarrow N_2 + HO_2 \qquad (13)$$

$$OH^* + N_2O \rightarrow HNO + NO \qquad (14)$$

However, at high ratios $[N_2O]/[H_2O]$, reactions 13 and 14, if occur, would lead to formation of reactive species HO_2 and HNO, which react with OH faster than the self-reaction 1a (k_{13} = 1.1×10^{-10}, $k_{14} = 1.5\times10^{-11}$ cm^3 $molecule^{-1}$ s^{-1}.[61]

To address this issue, we performed measurements of the yield of hydroxyl radicals after completion of all fast processes (reactions of $O(^1D)$, relaxation and other reactions of hot species) over a wide range of the $[N_2O]/H_2O]$ ratios. The relaxation processes as well as the processes 13 and 14 occur on the microsecond and sub-microsecond time scales and should manifest themselves in a decrease of the apparent yield of hydroxyl radicals at high $[N_2O]/[H_2O]$ ratios. The measurements were performed at three pressures, 1 bar, 0.1 bar and 0.01 bar (He). The results are shown in Fig. 7. At 0.01 bar, the ratio $[N_2O]/[H_2O]$ vas varied over a wide range, from 0.048 to 3.6 (75 times). No dependence was found for all three pressures, 0.01, 0.1 and 1 bar. The measured initial OH concentrations correspond to the predictions of the model, which does not include "hot" radical reactions (which includes translationally hot, as well as vibrationally and rotationally excited radicals) within the accuracy of the experimentally measured cross-sections. These experiments unambiguously demonstrate that reactions 13 and 14, as well as similar reactions, do not play any role under the experimental conditions of this and previous studies, and rule out the possibility of the explanation of the observed discrepancy in k_{1a} measurements due to the reactions of "hot" species.

The second issue is the treatment of the "out-of-beam" diffusion in Ref.[29, 49] The photolysis region has no axial symmetry, moreover, the region itself as well as the homogeneity of the photolysis light were ill defined. The diffusion contribution was not explicitly calculated in these studies, but rather was used as a fitting parameter. However, the "out-of-beam" contribution was not negligible or small. The contribution itself was of the order of the decay constant due to the chemical reaction. For example, in Fig. 2 of Ref.[49] the initial slope of the decay profile corresponds to 127 s^{-1}. Variation of the "diffusion loss constant" from 95 to 84 sec^{-1} lead to the large variation of the returned rate constant k_{1a} from $1.0x10^{-12}$ to $2.5x10^{-12}$ cm^3 $molecule^{-1}$ s^{-1}. However, the model curves that correspond to these parameters are almost indistinguishable. Then the choice of the proper diffusion loss rate constant was made based on the goodness of the fit. In the model used, diffusion contribution was approximated by a first order process. Under such an assumption, there are no expectations that the experimental profiles would be exactly reproduced, and the goodness of the fit by no means could be a criterion of the validity of the (strongly correlated) fitting parameters. The concentration temporal profiles due to the spreading by the diffusion are not exponential. Moreover, the diffusion spreading leads to the decrease of the concentration of the reactive species, which would further complicate the modeling of the second order reactions.

Another important observation in the studies of reaction 1a is the peculiar V-shaped temperature dependence. As it was pointed out previously and confirmed in the current study, the temperature dependence of the title reaction 1a is V-shaped, the rate decreases with temperature at low temperatures and starts increasing at about 427 K. The peculiar temperature dependence as well as the status of the theory in this respect require some discussion.

There have been several theoretical studies of the title reaction 1a. These studies are reviewed in the most recent paper of Nguyen and Stanton.[74] As it summarized in Ref.[74], all theoretical studies resulted in a *positive* barrier in reaction 1a, in the sense that the barrier top lies above the ground state energy of the reactants. Specifically, in Ref.[74] the calculated barrier height is +1.12 kcal/mol. In this respect, the experimentally observed negative temperature dependence at low temperatures (as well as the V-shaped temperature dependence over the wide temperature range) requires discussion. For a sequence of "simple metathesis reactions" of H-atom abstraction from HBr by small hydrocarbon free radicals (CH_3, C_2H_5, etc.) and some other radicals (e.g., SiH_3),[75-79] the observed negative temperature dependences were naturally

explained based on the fact that the top of the reaction barrier lies below the ground energy of the reactants (dubbed as "negative barriers", or could be called "submerged barriers" as suggested by J. Troe) on the example of the simplest reaction of this class, CH_3+HBr → CH_4 + Br. The theory based on the "negative barriers" also naturally predicts the V-shaped temperature dependence as well as possible pressure dependence presumably at very high pressures The structure of the Potential Energy Surface for such reactions (the top of the barrier below the reactants level, or, in more general terms, the "ground state" of the reaction bottleneck is below the reactant energy level) is crucial for the explanation of the negative temperature dependence at low temperatures as well as the V-shape.

In Ref.[74], the negative temperature dependence of k_{1a} at low and moderate temperature as well as the V-shaped temperature dependence over the wide temperature range was explained via the tunneling effects even for a positive barrier. Essentially, the approach is based on the existence of the "pre-reactive complex" (with the bonding energy of 3.37 kcal/mol.[74]) Qualitatively, it is clear that the pressure dependence of k_{1a} should have two limiting regimes, the "high pressure limit" when the pre-reactive complex is populated down to its ground state due to the stabilizing collisions with the bath gas molecules, and the "low pressure limit", when the collisions with the bath gas molecules are so scarce so that the pre-reaction complex is not populated below the reactants zero energy at all. As it was estimated for a similar reaction in Ref.[78] and correctly indicated in Ref.[74], the "high pressure" regime requires very high pressures (compared to the pressures employed in the experimental studies of reaction 1a). Then all calculations must be done for the "low pressure" limit, when the pre-reactive complex is not populated at all at the energies below the ground state of the reactants (zero energy). Even very simple estimates show that the experimental conditions used to study reaction 1a are several orders of magnitude down into the "low pressure" region. For estimates, using the "gas collision" rate constant of $5x10^{-10}$ cm^3 $molecule^{-1}$ s^{-1} and the rate constant $k_{1a}=1.4x10^{-12}$ cm^3 $molecule^{-1}$ s^{-1}, for the probability of a reactive collision of OH + OH one obtains $1.4x10^{-12}/5x10^{-10} = 2.8x10^{-3}$. Estimating the deactivation rate constant in the collisions with the bath gas molecules of $5x10^{-11}$ cm^3 $molecule^{-1}$ s^{-1} (weak collisions, $\beta c=0.1$), bath gas density of $3.3x10^{16}$ molecule cm^{-3} (1 Torr), the stabilization rate of the collision complex would be $3.3x10^{16}x5x10^{-11} = 1.7x10^6$ s^{-1}. Roughly estimating the lifetime of the activated pre-collision complex as 3 nm/$3x10^4$ m/s = 10^{-13} s, for the probability of the collision pre-reactive complex to be stabilized in a single binary OH + OH

collision is $1x10^{-13}x1.7x10^{6} = 1.7x10^{-7}$, which is more than 4 orders smaller than the probability to react. More accurate estimate of the lifetime of the excited pre-reactive complex might somewhat change this estimate. In any case, the issue is the value of the rate constant in the "low pressure" regime, which is to be compared with the experiment.

In Ref.[74], the V-shape of the temperature dependence is assigned to the peculiar temperature dependence of the tunneling factor, which presumably decreases with temperature faster than the increase of the classical TST rate constant. Such a behavior of the rate constant is counterintuitive, and there are some other questionable outcomes of the calculations. The calculations results indicate that at low temperatures (e.g. 200 K) the tunneling factor is about a factor of 11, which means that ca. 90% reaction proceeds below the reaction barrier, i.e., by tunneling. In such a case, isotope substitution H → D must have a strong impact on the tunneling probability. However, the calculations result only in ca. 20% drop of the tunneling factor for OD+OD reaction compared to that for OH+OH reaction at 200 K. Unfortunately, only a few details on the tunneling calculations are given,[74] obviously, further theoretical work is required to explain the peculiar temperature dependence of the title reaction.

Conclusions

The rate constant of the disproportionation channel of the self-reaction of hydroxyl radicals (reaction 1a) was measured at ambient temperature using two different experimental techniques (pulsed laser photolysis coupled to transient UV absorption and the discharge fast flow reactor coupled to mass-spectrometric detection) and three different techniques of generation of hydroxyl radicals. All three studies are in excellent agreement, and unambiguously confirm the lower value of the rate constant of the title reaction of $k_{1a} = (1.4 \pm 0.2)\times10^{-12}$ cm^3 molecule^{-1} s^{-1} (298 ± 5 K). In addition, the reaction was studied over an extended temperature range 220 – 950 K using discharge fast flow – MS technique. This study confirmed the V-shaped temperature dependence with the turning point at 427 K, in excellent agreement with the previous studies of the NJIT group.[36, 50]

Acknowledgement

This work is partially supported by the National Science Foundation under Grant No. CBET-0827398 and by the Russian Science Foundation under Project 19-73-20060. The study

performed at IChK&C (Novosibirsk) was supported by a grant from the Russian Science Foundation (Grant No. 19-73-20060).

Associated Content

Supporting Information. Sample ozone depletion profile (Figure S1), the diagram of the high temperature flow reactor (Figure S2), sample OH profile in photolysis of ozone containing mixtures (Figure S3), examples of the kinetics of OH loss at different temperatures (Figures S4, S5), the reaction mechanism which was used in the fitting the experimental profiles (Table S1).

Table 1. Summary of the measurements of the rate constants of the reaction OH + OH → O + H_2O (1a) using discharge fast flow coupled with mass-spectrometry technique (ICARE, Orleans).

T (K)	No./exp.[a]	$[OH]_0$ [b]	k_7 [c]	k_{1a} [d]
220	27	0.49-32.2	10.4, 18.0	2.10
238	9	0.49-33.7	16.4	2.00
260	27	0.48-38.6	5.1, 9.3	1.79
286	12	0.43-26.7	5.7	1.55
295	11	1.24-40.0	4.6	1.48
318	10	0.87-40.3	4.0	1.41
360	11	0.85-35.2	4.1	1.34
410	13	0.77-33.8	4.7	1.28
480	15	0.64-35.0	9.8	1.22
586	14	0.38-46.7	15.1	1.33
718	15	0.39-42.1	15.9	1.48
823	16	0.36-35.6	17.6	1.78
950	17	0.35-29.6	27.6	2.11

[a] Number of kinetic runs. [b] Units of 10^{12} molecule cm^{-3}. [c] Units of s^{-1}, [d] Units of 10^{-12} cm^3 $molecule^{-1}$ s^{-1}, estimated uncertainty on k_{1a} is nearly 15%. [d] Units of 10^{-12} cm^3 $molecule^{-1}$ s^{-1}, estimated statistical and total uncertainties on k_1 are ≤ 10% and about 15%, respectively.

Figure Captions

Figure 1. Sample UV absorption profiles of OH radical (multiline at ca. 308 nm). Photolysis of N_2O/H_2O/He mixture at 193.3 nm. T = 295 K, p = 0.01 bar (7.51 Torr). $[N_2O] = 1.54x10^{16}$ molecule cm^{-3}, $H_2O = 1.57x10^{17}$ molecule cm^{-3}, $[N_2O] / [H_2O] = 0.1$. The initial concentration of OH is varied by the laser light attenuation. Wall coating PFPE (Krytox 1525). Black – experimental curve, yellow – fitting, magenta – the residual of the fit. The red and green curves are the experimental profiles obtained at the same experimental conditions using attenuated laser light.

Figure 2. The initial slope analysis ("the first approximation") of a series of measurements at 295 K, 0.01 bar (He). The reactants concentrations are kept constant (as in Fig. 1), the initial concentration is varied by attenuation of the laser light using meshes and quartz plates. The fraction of the decay curves starting at 1.2 ms until ca. 1/3 of the amplitude decay is fitted with an exponential function to determine the "initial slope" rate constant. Wall coating PFPE (Krytox 1525). The results: the intercept = 35.4 s^{-1}, calculated wash-out time = 145 cm/s/10 cm = 14.5 s^{-1}, then the first approximation $k_{w,OH}$ = 21 s^{-1}. Assuming the apparent stoichiometric coefficient of 3.37 for these experimental conditions (obtained using modeling of the kinetic absorption profiles using the complete model (see text) results in the first approximation rate constant for the channel 1a of $k_{1a}= 1.40x10^{-12}$ cm^3 $molecule^{-1}$ s^{-1}.

Figure 3. The final iteration (3^{rd}) in the processing of a series of measurements. Wall coating PFPE (Krytox 1525). The original absorption profiles are fitted using full kinetic model by numerical solution of the ODE system corresponding to the reaction mechanism using SCIENTIST software (see text). The first approximation wall rate constant obtained via the "initial slope" analysis (Fig. 2) is used in the reaction model. The wash-out contribution is explicitly installed in the fitting model. The resulting product $k1a[OH]_{ini}$ is plotted vs. $[OH]_{ini}$, the intercept is used to adjust the wall decay rate constant, $k_{w,OH}$, until the intercept becomes zero. In this example, the procedure converged in two additional steps beyond the initial slope analysis, yielding the rate constant k_{1a} of $1.39x10^{-12}$ cm^3 $molecule^{-1}$ s^{-1}.

Figure 4. Sample data processing for the experiments with photolysis of ozone at 266 nm as a source of excited oxygen atoms, $O(^1D)$. Mixtures of $O_3/O_2/H_2O$/He are photolysed using the 4th harmonic of Nd:YAG laser (266 nm). The presence of molecular oxygen is due to the incomplete conversion to ozone in the inline dielectric barrier discharge ozonator. The plot shows the last iteration of the iterative procedure as described above for the N_2O + 193 nm experiments. The reactor walls as well as the windows are coated with Halocarbon Wax. The wall decay rate constant, $k_{w,OH}$ = 15 s^{-1}, the returned rate constant k1a = (1.34 ± 0.10)x10^{-12} cm^3 $molecule^{-1}$ s^{-1} (± 3 σ). Circles: obtained by processing the OH decay profiles. Squares: obtained by processing the O_3 profiles (partial decay due to the reaction OH + O_3).

Figure 5. Examples of the temporal profiles of OH radicals observed at T = 220 (a) and 950 K (b) with different initial concentrations of the radicals. Solid lines correspond to the fit to the experimental data using Eq. 2. Partially shown error bars represent maximum uncertainty of 5% on the measurements of relative concentrations of OH.

Figure 6. Summary of the temperature dependent measurements of k_{1a}. The error bars correspond to estimated 15% uncertainty on the measurements of k_{1a} in the present work; uncertainties on previous measurements are given as reported in respective studies. The dashed lines correspond to the ± 20% deviation from the expression E4 (black line), showing that almost all experimental points fall within these limits (see text).

Figure 7. The yield of OH radicals vs. $[N_2O]/[H_2O]$ ratio at 0.01 bar (a), 0.1 bar (b) and 1 bar (c). At 0.01 bar the $[N_2O]/[H2O]$ ratio is varied from 0.048 to 3.6 (75 times).

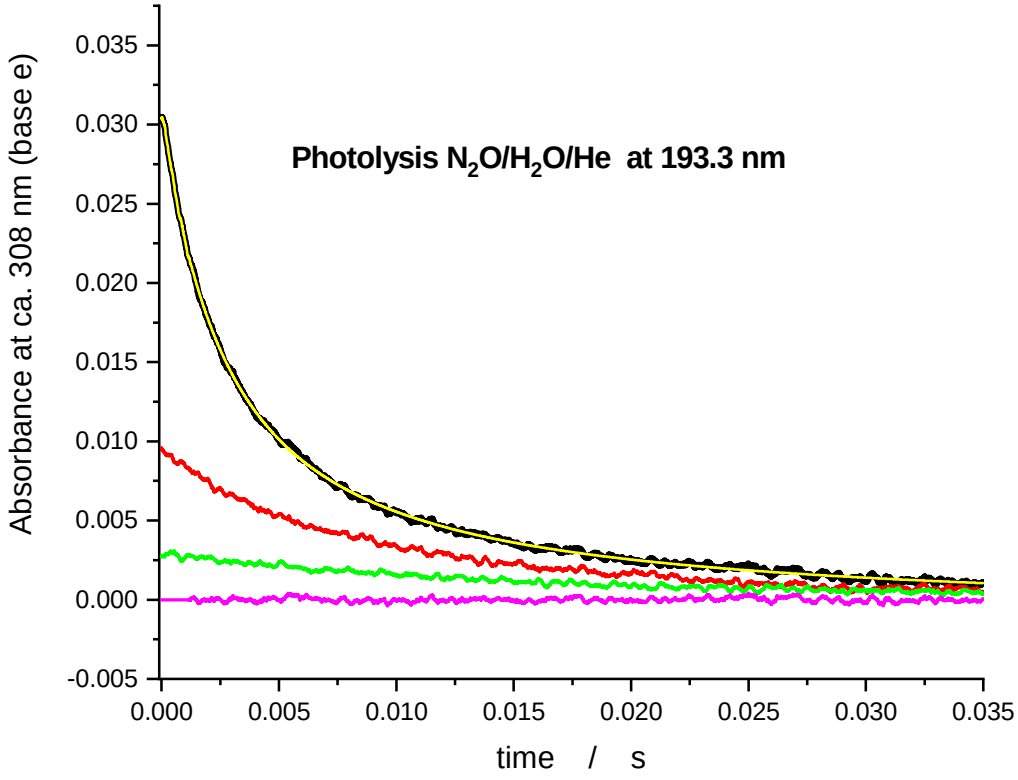

Figure 1. Sample UV absorption profiles of OH radical (multiline at ca. 308 nm). Photolysis of N_2O/H_2O/He mixture at 193.3 nm. T = 295 K, p = 0.01 bar (7.51 Torr). $[N_2O] = 1.54 \times 10^{16}$ molecule cm^{-3}, $H_2O = 1.57 \times 10^{17}$ molecule cm^{-3}, $[N_2O] / [H_2O] = 0.1$. The initial concentration of OH is varied by the laser light attenuation. Wall coating PFPE (Krytox 1525). Black – experimental curve, yellow – fitting, magenta – the residual of the fit. The red and green curves are the experimental profiles obtained at the same experimental conditions using attenuated laser light.

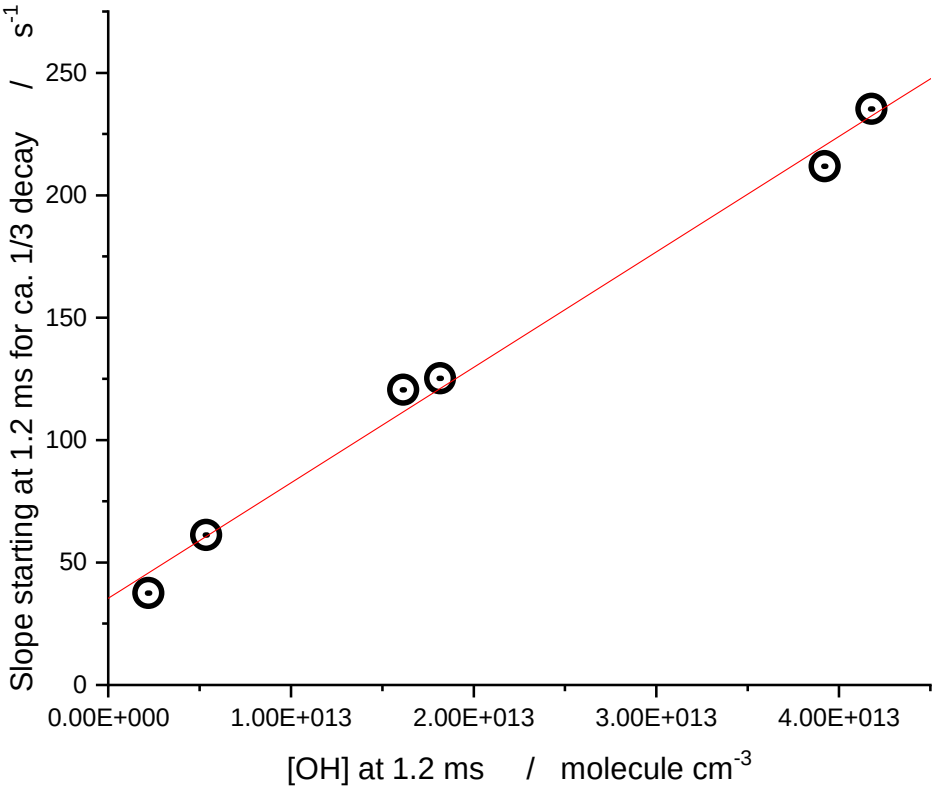

Figure 2. The initial slope analysis ("the first approximation") of a series of measurements at 295 K, 0.01 bar (He). The reactants concentrations are kept constant (as in Fig. 1), the initial concentration is varied by attenuation of the laser light using meshes and quartz plates. The fraction of the decay curves starting at 1.2 ms until ca. 1/3 of the amplitude decay is fitted with an exponential function to determine the "initial slope" rate constant. Wall coating PFPE (Krytox 1525). The results: the intercept = 35.4 s^{-1}, calculated wash-out time = 145 cm/s/10 cm = 14.5 s^{-1}, then the first approximation $k_{w,OH}$ = 21 s^{-1}. Assuming the apparent stoichiometric coefficient of 3.37 for these experimental conditions (obtained using modeling of the kinetic absorption profiles using the complete model (see text)) results in the first approximation rate constant for the channel 1a of k_{1a}= 1.40x10^{-12} cm^3 $molecule^{-1}$ s^{-1}.

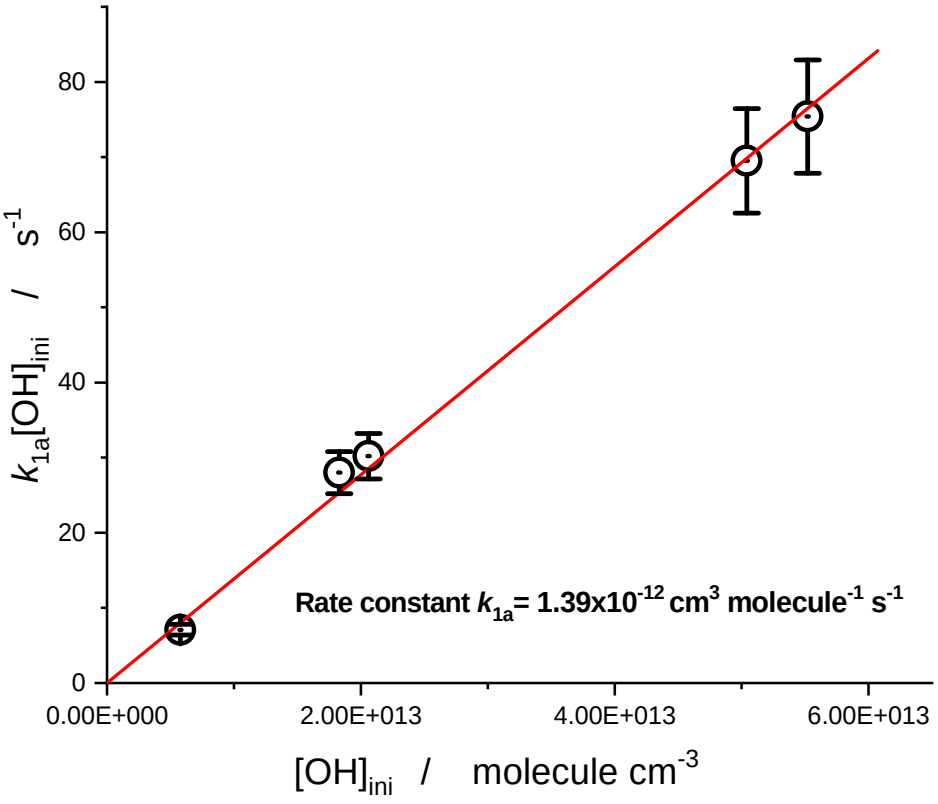

Figure 3. The final iteration (3[rd]) in the processing of a series of measurements. Wall coating PFPE (Krytox 1525). The original absorption profiles are fitted using full kinetic model by numerical solution of the ODE system corresponding to the reaction mechanism using SCIENTIST software (see text). The first approximation wall rate constant obtained via the "initial slope" analysis (Fig. 2) is used in the reaction model. The wash-out contribution is explicitly installed in the fitting model. The resulting product $k_{1a}[OH]_{ini}$ is plotted vs. $[OH]_{ini}$, the intercept is used to adjust the wall decay rate constant, $k_{w,OH}$, until the intercept becomes zero. In this example, the procedure converged in two additional steps beyond the initial slope analysis, yielding the rate constant k_{1a} of 1.39x10^{-12} cm^3 molecule^{-1} s^{-1}.

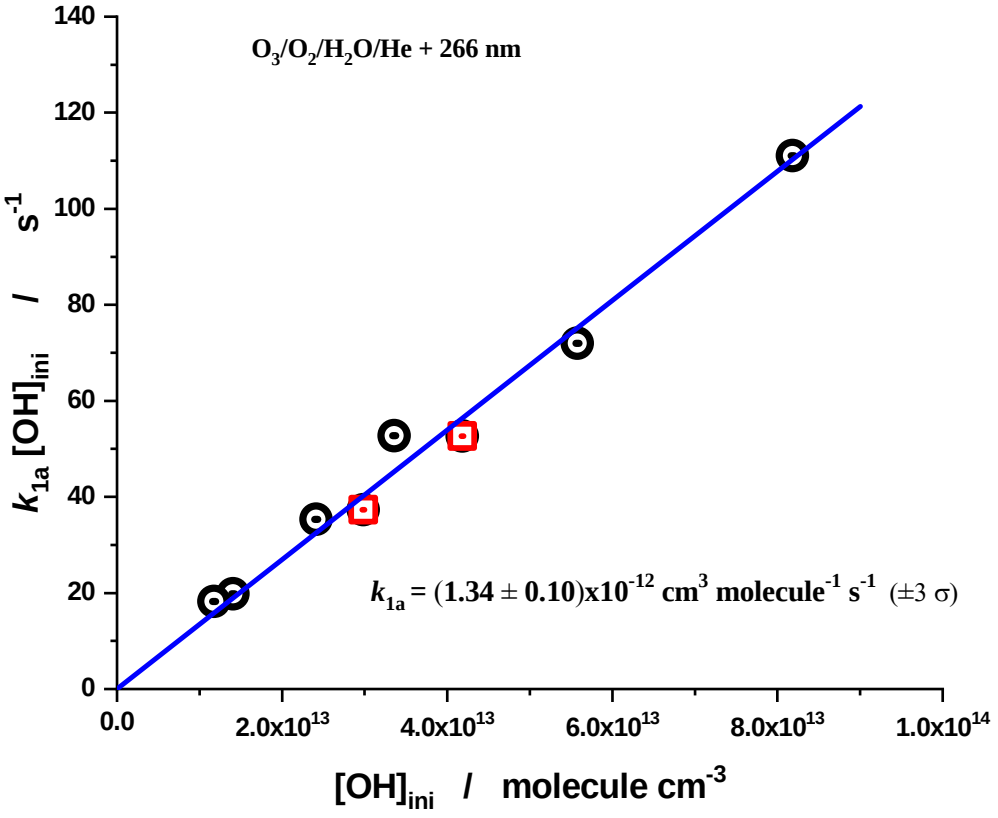

Figure 4. Sample data processing for the experiments with photolysis of ozone at 266 nm as a source of excited oxygen atoms, O(^{1}D). Mixtures of $O_3/O_2/H_2O$/He are photolyzed using the 4th harmonic of Nd:YAG laser (266 nm). The presence of molecular oxygen is due to the incomplete conversion to ozone in the inline dielectric barrier discharge ozonator. The plot shows the last iteration of the iterative procedure as described above for the N_2O + 193 nm experiments. The reactor walls as well as the windows are coated with Halocarbon Wax. The wall decay rate constant, $k_{w,OH}$ = 15 s^{-1}, the returned rate constant k_{1a} = (1.34 ± 0.10)x10^{-12} cm^3 molecule^{-1} s^{-1} (± 3 σ). Circles: obtained by processing the OH decay profiles. Squares: obtained by processing the O_3 profiles (partial decay due to the reaction OH + O_3).

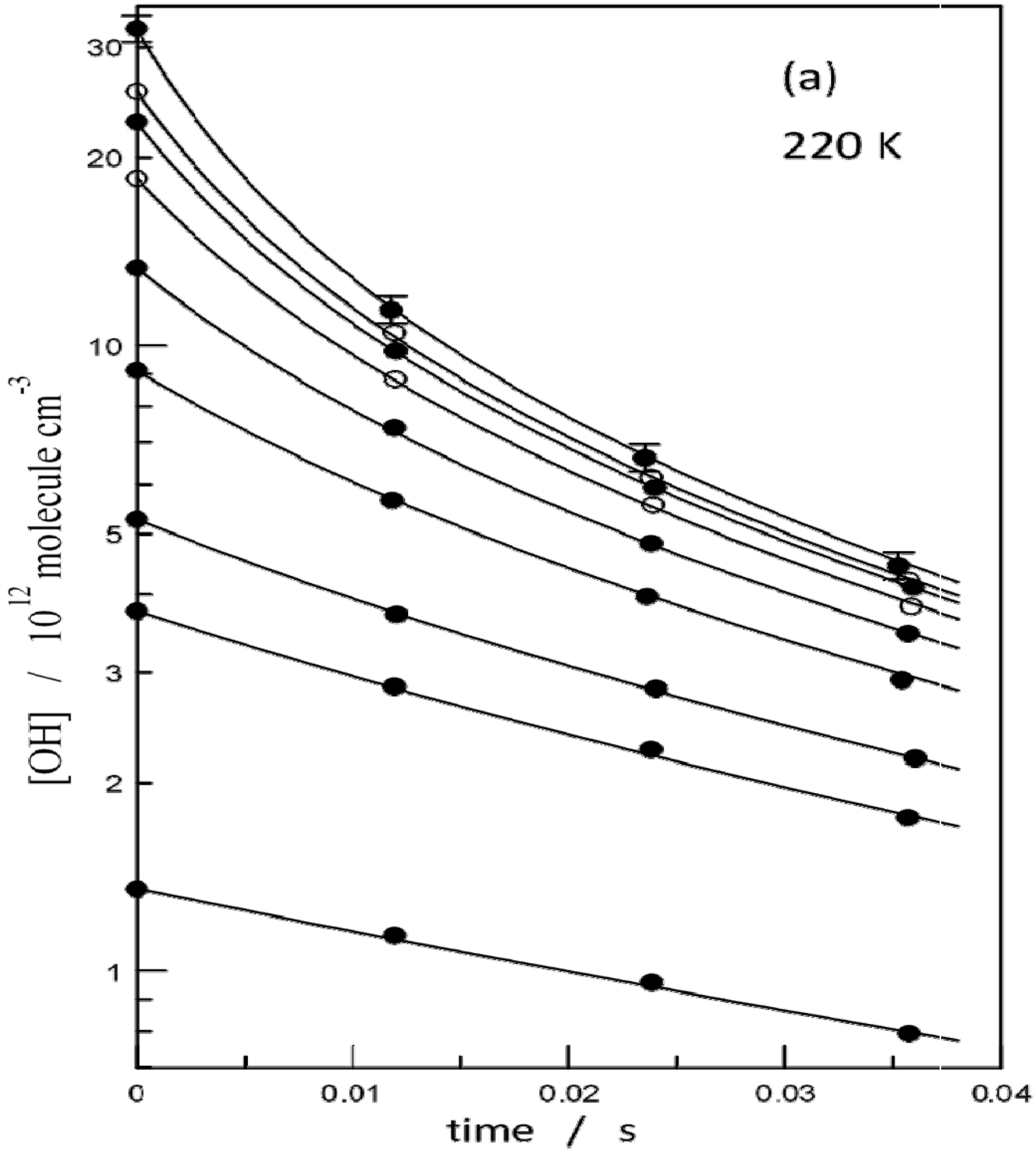
(a)
220 K
[OH] / 10^12 molecule cm^-3
time / s
30
20
10
5
3
2
1
0
0.01
0.02
0.03
0.04

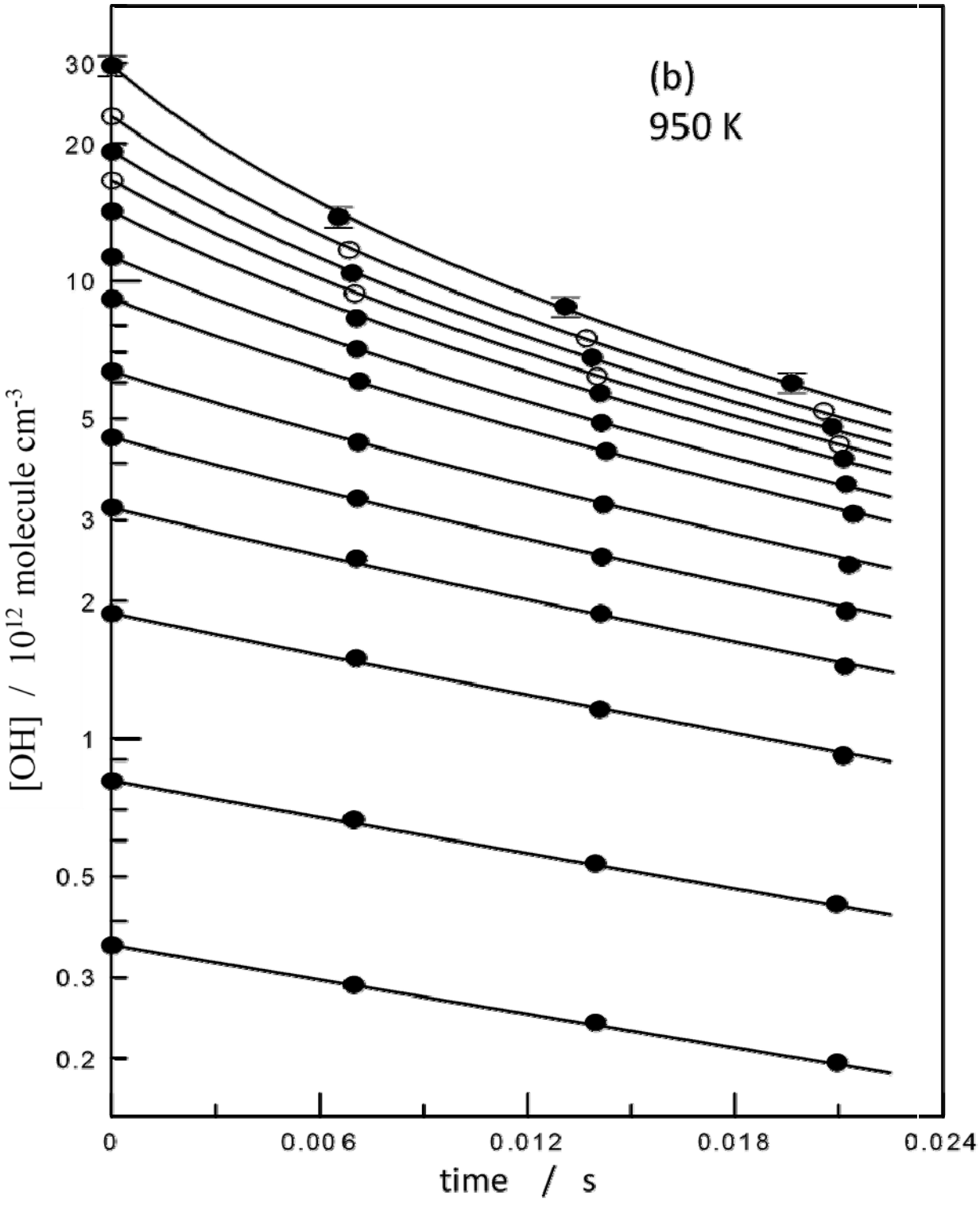
(b)
950 K
30
20
10
5
3
2
1
0.5
0.3
0.2
[OH] / 10^{12} molecule cm^{-3}
0
0.006
0.012
0.018
0.024
time / s

Figure 5. Examples of the temporal profiles of OH radicals observed at T = 220 (a) and 950 K (b) with different initial concentrations of the radicals. Solid lines correspond to the fit to the experimental data using equation E2. Partially shown error bars represent maximum uncertainty of 5% on the measurements of relative concentrations of OH.

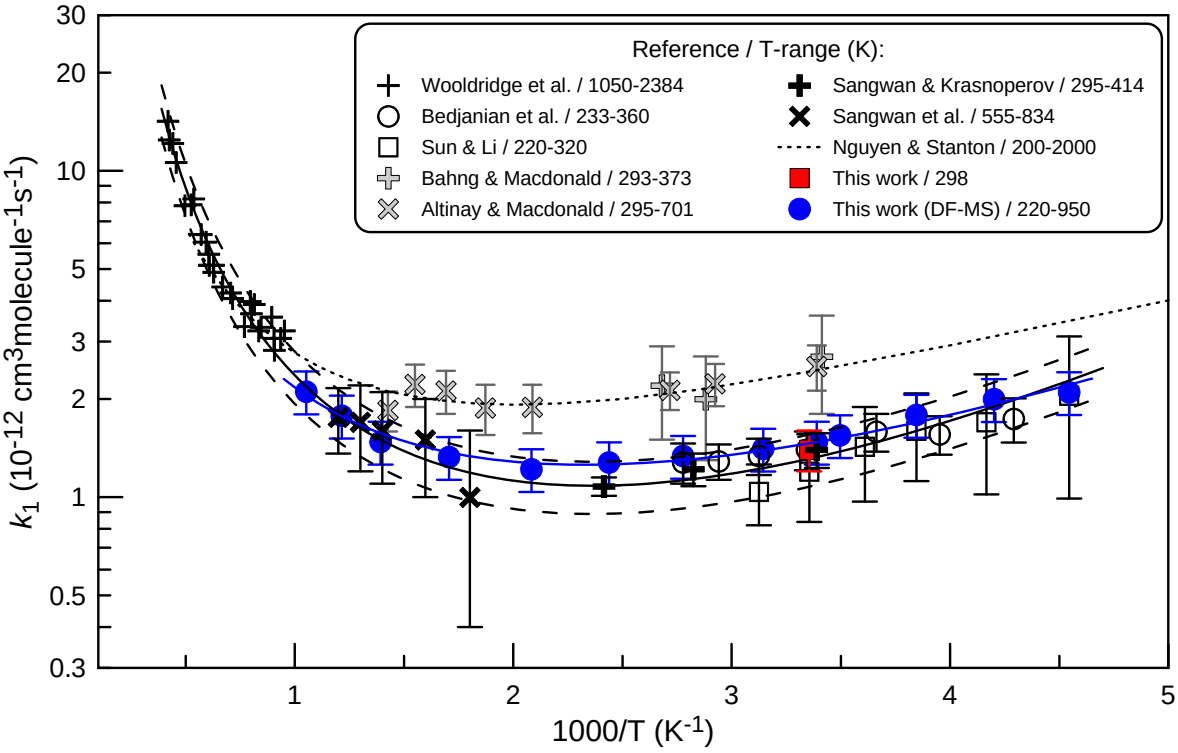

Figure 6. Summary of the temperature dependent measurements of k_{1a}. The error bars correspond to estimated 15% uncertainty on the measurements of k_{1a} in the present work; uncertainties on previous measurements are given as reported in respective studies. The dashed lines correspond to the ± 20% deviation from the expression E4 (black line), showing that almost all experimental points fall within these limits (see text).

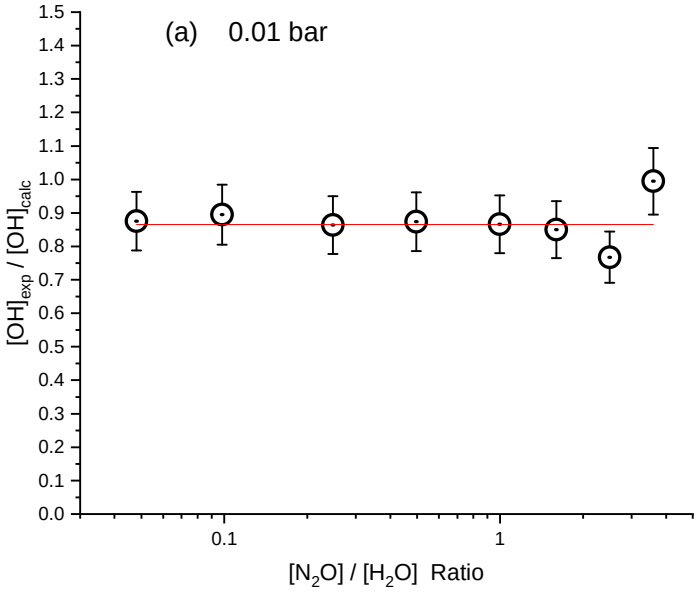
(a) 0.01 bar
[OH]exp / [OH]calc
1.5
1.4
1.3
1.2
1.1
1.0
0.9
0.8
0.7
0.6
0.5
0.4
0.3
0.2
0.1
0.0
0.1
1
[N2O] / [H2O] Ratio

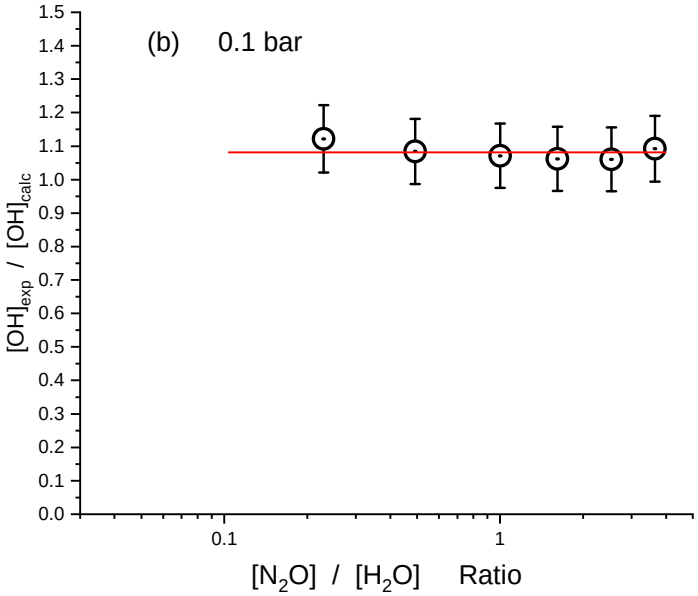
(b) 0.1 bar
[OH]exp / [OH]calc
1.5
1.4
1.3
1.2
1.1
1.0
0.9
0.8
0.7
0.6
0.5
0.4
0.3
0.2
0.1
0.0
0.1
1
[N2O] / [H2O] Ratio

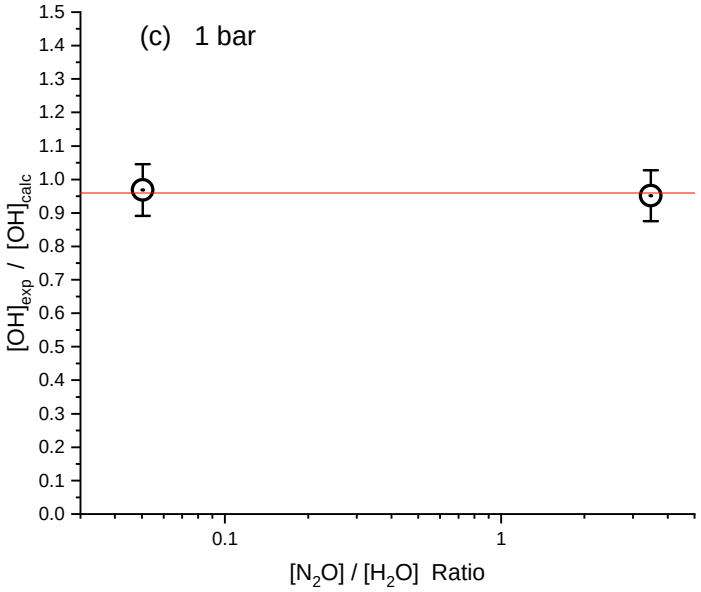

Figure 7. The yield of OH radicals vs. $[N_2O]/[H_2O]$ ratio at 0.01 bar (a), 0.1 bar (b) and 1 bar (c). At 0.01 bar the $[N_2O]/[H_2O]$ ratio is varied from 0.048 to 3.6 (75 times).

References

1. Atkinson, R. Kinetics and Mechanisms of the Gas-Phase Reactions of the Hydroxyl Radical with Organic Compounds Under Atmospheric Conditions. *Chem. Rev.* **1986,** *86*, 69-201.
2. Lelieveld, J.; Dentener, F. J.; Peters, W.; Krol, M. C. On the Role of Hydroxyl Radicals in the Self-Cleansing Capacity of the Troposphere. *Atmos. Chem. Phys.* **2004,** *4*, 2337-2344.
3. Finlayson-Pitts, B. J.; Pitts, J. N. Tropospheric Air Pollution: Ozone, Airborne Toxics, Polycyclic Aromatic Hydrocarbons, and Particles. *Science* **1997,** *276*, 1045-1051.
4. Calvert, J. G.; Derwent, R. J.; Orlando, J. J.; Tyndall, J. S.; Wallington, T. J., Mechanisms of Atmospheric Oxidation of the Alkanes. *Oxford University Press US*: 2008.
5. Ravishankara, A. R. Kinetics of Radical Reactions in the Atmospheric Oxidation of Methane. *Annu. Rev. Phys. Chem.* **1988,** *39*, 367-394.
6. Montzka, S. A.; Krol, M.; Dlugokencky, E.; Hall, B.; Jöckel, P.; Lelieveld, J. Small Interannual Variability of Global Atmospheric Hydroxyl. *Science* **2011,** *331*, 67-69.
7. Smith, I. W. M.; Ravishankara, A. R. Role of Hydrogen-Bonded Intermediates in the Bimolecular Reactions of the Hydroxyl Radical. *J. Phys. Chem. A* **2002,** *106*, 4798-4807.
8. Smith, R. H. Role of Hydroxyl Radicals in Combustion. *Coal Research in CSIRO* **1967,** *No. 32*, 9-18.
9. Westbrook, C. K. Chemical Kinetics of Hydrocarbon Ignition in Practical Combustion Systems. *Proc. Combust. Inst.* **2000,** *28*, 1563-1577.
10. Miller, J. A.; Pilling, M. J.; Troe, J. Unravelling Combustion Mechanisms Through a Quantitative Understanding of Elementary Reactions. *Proc. Combust. Inst.* **2005,** *30*, 43-88.
11. Warnatz, J. The Mechanism of High Temperature Combustion of Propane and Butane. *Combust. Sci. Technol.* **1983,** *34*, 177-200.
12. Haber, F. Combustion and Explosion Processes. *Angew. Chem.* **1929,** *42*, 745-751.
13. Kondrat'ev, V. N. Free Hydroxyl. *Usp. Khim.* **1939,** *8*, 195-240.
14. Tsang, W. The Combustion Kinetics of Real Fuels. *Chem. Phys. Processes Combust.* **2009**, tsang1/1-tsang1/9.
15. Kaufman, F.; Del Greco, F. P. Fast Reactions of OH Radicals. *Symp. (Int.) Combust., [Proc.]* **1962**, 659-66, discussion 666-8.
16. Caldwell, J.; Back, R. A. Combination Reactions of Hydroxyl Radicals in the Flash Photolysis of Water Vapor. *Trans. Faraday Soc.* **1965,** *61*, 1939-1945.
17. Dixon-Lewis, G.; Wilson, W. E.; Westenberg, A. A. Studies of Hydroxyl Radical Kinetics by Quantitative E.S.R. *J. Chem. Phys.* **1966,** *44*, 2877-2884.
18. Wilson, W. E., Jr.; O'Donovan, J. T. Mass-Spectrometric Study of the Reaction Rate of Hydroxide with Itself and with Carbon Monoxide. *J. Chem. Phys.* **1967,** *47*, 5455-5457.
19. Mulcahy, M. F. R.; Smith, R. H. Reactions of OH Radicals in the Hydrogen-Nitrogen Dioxide and Hydrogen-Nitrogen Dioxide-Carbon Monoxide Systems. *J. Chem. Phys.* **1971,** *54*, 5215-5221.
20. McKenzie, A.; Mulcahy, M. F. R.; Steven, J. R. Kinetics of Decay of Hydroxyl Radicals at Low Pressure. *J. Chem. Phys.* **1973,** *59*, 3244-3254.
21. Westenberg, A. A.; DeHaas, N. Rate of the Reaction Hydroxide + Hydroxide to Water + Atomic Oxygen. *J. Chem. Phys.* **1973,** *58*, 4066-4071.
22. Clyne, M. A. A.; Down, S. Kinetics Behavior of Hydroxyl Radical $X^2\Pi$ and $A^2\Sigma^+$ Using Molecular Resonance Fluorescence Spectrometry. *J. Chem. Soc. Faraday Trans. 2* **1974,** *70*, 253-266.

23. Farquharson, G. K.; Smith, R. H. Rate Constants for the Gaseous Reactions Hydroxyl + Ethene and Hydroxyl + Hydroxyl. *Aust. J. Chem.* **1980,** *33*, 1425-1435.
24. Trainor, D. W.; Von Rosenberg, C. W., Jr. Flash Photolysis Study of the Gas Phase Recombination of Hydroxyl Radicals. *J. Chem. Phys.* **1974,** *61*, 1010-1015.
25. Zellner, R.; Ewig, F.; Paschke, R.; Wagner, G. Pressure and Temperature Dependence of the Gas-Phase Recombination of Hydroxyl Radicals. *J. Phys. Chem.* **1988,** *92*, 4184-4190.
26. Wagner, G.; Zellner, R. Temperature Dependence of the Reaction Hydroxyl + Hydroxyl → Water + Atomic Oxygen. *Ber. Bunsenges. Phys. Chem.* **1981,** *85*, 1122-1128.
27. Bedjanian, Y.; Le Bras, G.; Poulet, G. Kinetic Study of OH + OH and OD + OD Reactions. *J. Phys. Chem. A* **1999,** *103*, 7017-7025.
28. Sun, H.; Li, Z. Rate Constant Measurement for the OH+OH→H_2O+O reaction at 220–320 K Using Discharge Flow/Mass Spectrometer/Resonance Fluorescence Technique. *Chem. Phys. Lett.* **2004,** *399*, 33-38.
29. Bahng, M.-K.; Macdonald, R. G. Determination of the Rate Constant for the OH($X^2\Pi$) + OH($X^2\Pi$) → O(^{3}P) + H_2O Reaction over the Temperature Range 293-373 K. *J. Phys. Chem. A* **2007,** *111*, 3850-3861.
30. Forster, R.; Frost, M.; Fulle, D.; Hamann, H. F.; Hippler, H.; Schlepegrell, A.; Troe, J. High Pressure Range of the Addition of HO to HO, NO, NO_2, and CO. I. Saturated Laser Induced Fluorescence Measurements at 298 K. *J. Chem. Phys.* **1995,** *103*, 2949-2958.
31. Fulle, D.; Hamann, H. F.; Hippler, H.; Troe, J. Temperature and Pressure Dependence of the Addition Reactions of HO to NO and to NO_2. IV. Saturated Laser-Induced Fluorescence Measurements up to 1400 bar. *J. Chem. Phys.* **1998,** *108*, 5391-5397.
32. Ernst, J.; Wagner, H. G.; Zellner, R. Direct Rate Measurements for OH + OH —> H_2O + O in the Range 1200-1800 K. *Ber. Bunsenges. Phys. Chem.* **1977,** *81*, 1270–1275.
33. Wooldridge, M. S.; Hanson, R. K.; Bowman, C. T. A Shock Tube Study of the OH + OH → H_2O + O Reaction. *Int. J. Chem. Kinet.* **1994,** *26*, 389-401.
34. Sutherland, J. W.; Patterson, P. M.; Klemm, R. B. Rate Constants for the Reaction, Oxygen Atom O(^{3}P) + water <=> Hydroxyl + Hydroxyl, over the Temperature Range 1053 K to 2033 K using two Direct Techniques. *Symp. (Int.) Combust., [Proc.]* **1991,** *23rd*, 51-57.
35. Sangwan, M.; Chesnokov, E. N.; Krasnoperov, L. N. Reaction CH_3 + OH Studied over the 294 - 714 K Temperature and 1 - 100 bar Pressure Ranges. *J. Phys. Chem. A* **2012,** *116*, 8661 - 8670.
36. Sangwan, M.; Chesnokov, E. N.; Krasnoperov, L. N. Reaction OH + OH Studied over the 298–834 K Temperature and 1 - 100 bar Pressure Ranges. *J. Phys. Chem. A* **2012,** *116*, 6282-6294.
37. Harding, L. B.; Wagner, A. F. Theoretical Study of the Reaction Rates of OH + OH <==> H_2O + O. *Symp. (Int.) Combust., [Proc.]* **1989,** *22nd*, 983-989.
38. Karkach, S. P.; Osherov, V. I. Ab Iinitio Analysis of the Transition States on the Lowest Triplet H_2O_2 Potential Surface. *J. Chem. Phys.* **1999,** *110*, 11918-11927.
39. Kuhn, B.; Rizzo, T. R.; Luckhaus, D.; Quack, M.; Suhm, M. A. A New Six-Dimensional Analytical Potential up to Chemically Significant Energies for the Electronic Ground State of Hydrogen Peroxide. *J. Chem. Phys.* **1999,** *111*, 2565-2587.
40. Brouwer, L.; Cobos, C. J.; Troe, J.; Duebal, H. R.; Crim, F. F. Specific Rate Constants k(E,J) and Product State Distributions in Simple Bond Fission Reactions. II. Application to Hydrogen Peroxide → Hydroxyl + Hydroxyl. *J. Chem. Phys.* **1987,** *86*, 6171-6182.

41. Maergoiz, A. I.; Nikitin, E. E.; Troe, J. Statistical Adiabatic Channel Calculation of Accurate Low-Temperature Rate Constants for the Recombination of OH Radicals in their Ground Rovibronic State. *J. Chem. Phys.* **1995,** *103*, 2083-2091.
42. Braunstein, M.; Panfili, R.; Shroll, R.; Bernstein, L. Potential Surfaces and Dynamics of the $O(^3P)+H_2O(X^1A_1)$ –→ $OH(X^2\Pi)+OH(X^2\Pi)$ Reaction. *J. Chem. Phys.* **2005,** *122*, 184307-184313.
43. Troe, J.; Ushakov, V. G. SACM/CT Study of the Dissociation/Recombination Dynamics of Hydrogen Peroxide on an *ab initio* Potential Energy Surface. Part II. Specific Rate Constants k(E,J), Thermal Rate Constants $k_{infin.}$(T), and Lifetime Distributions. *Phys. Chem. Chem. Phys.* **2008,** *10*, 3915-3924.
44. Harding, L. B. Theoretical Studies of the Hydrogen Peroxide Potential Surface. 2. An *ab initio*, Long-range, Hydroxyl($^2\Pi$) + Hydroxyl($^2\Pi$) Potential. *J. Phys. Chem.* **1991,** *95*, 8653-8660.
45. Sellevag, S. R.; Georgievskii, Y.; Miller, J. A. The Temperature and Pressure Dependence of the Reactions H + O_2 (+M) → HO_2 (+M) and H + OH (+M) → H_2O (+M). *J. Phys. Chem. A* **2008,** *112*, 5085-5095.
46. Deyerl, H.-J.; Clements, T. G.; Luong, A. K.; Continetti, R. E. Transition State Dynamics of the OH+OH → O+H_2O Reaction Studied by Dissociative Photodetachment of H_2O_2. *J. Chem. Phys.* **2001,** *115*, 6931-6940.
47. Atkinson, R.; Baulch, D. L.; Cox, R. A.; Crowley, J. N.; Hampson, R. F.; Hynes, R. G.; Jenkin, M. E.; Rossi, M. J.; Troe, J. Evaluated Kinetic and Photochemical Data for Atmospheric Chemistry: Volume I - Gas Phase Reactions of Ox, HOx, NOx and SOx Species. *Atmos. Chem. Phys.* **2004,** *4*, 1461-1738.
48. Atkinson, R.; Baulch, D. L.; Cox, R. A.; Hampson, R. F., Jr.; Kerr, J. A.; Rossi, M. J.; Troe, J. Evaluated Kinetic and Photochemical Data for Atmospheric Chemistry, Organic Species: Supplement VII. *J. Phys. Chem. Ref. Data* **1999,** *28*, 191-393.
49. Altinay, G.; Macdonald, R. G. Determination of the Rate constant for the OH($X^2\Pi$) + OH($X^2\Pi$) → H_2O + O(^3P) Reaction over the Temperature Range 295 to 701 K. *J. Phys. Chem. A* **2014,** *118*, 38-54.
50. Sangwan, M.; Krasnoperov, L. N. Disproportionation Channel of Self-Reaction of Hydroxyl Radical, OH + OH → H_2O + O, Studied by Time-Resolved Oxygen Atom Trapping. *J. Phys. Chem. A* **2012,** *116*, 11817-11822.
51. Grebenkin, S. Y.; Krasnoperov, L. N. Kinetics and Thermochemistry of the Hydroxycyclohexadienyl Radical Reaction with O_2: C_6H_6OH + O2 <=> $C_6H_{6(}OH)OO$. *J. Phys. Chem. A* **2004,** *108*, 1953-1963.
52. Krasnoperov, L. N.; Chesnokov, E. N.; Stark, H.; Ravishankara, A. R. Unimolecular Dissociation of Formyl Radical, HCO –→ H + CO, Studied Over 1 - 100 bar Pressure Range. *J. Phys. Chem. A* **2004,** *108*, 11526-11536.
53. Krasnoperov, L. N.; Chesnokov, E. N.; Stark, H.; Ravishankara, A. R. Elementary Reactions of Formyl (HCO) Radical Studied by Laser Photolysis - Transient Absorption Spectroscopy. *Proc. Combust. Inst.* **2005,** *30*, 935-943.
54. Greenblatt, G. D.; Ravishankara, A. R. Laboratory Studies on the Stratospheric NOx Production Rate. *J. Geophys. Res.* **1990,** *95*, 3539-3547.
55. Butler, J. E.; Talley, L. D.; Smith, G. K.; Lin, M. C. Rotational and Vibrational Energy Distributions of Hydroxyl Radical (Oxygen-16)($X^2\Pi$) and Hydroxyl Radical (Oxygen-18)($X^2\Pi$)

Produced in the Reaction of Atomic Oxygen(^{1}D) with Water and Water(Oxygen-18). *J. Chem. Phys.* **1981,** *74*, 4501-4508.
56. Sauder, D. G.; Stephenson, J. C.; King, D. S.; Casassa, M. P. Nascent Product States in the Photoinitiated Reaction of Ozone with Water. *J. Chem. Phys.* **1992,** *97*, 952-961.
57. Tanaka, N.; Takayanagi, M.; Hanazaki, I. Nascent Rotational and Vibrational Distributions in ^{16}OH and ^{18}OH Produced in the Reaction of O(^{1}D) with $H_2{}^{18}O$. *Chem. Phys. Lett.* **1996,** *254*, 40-46.
58. Sander, S. P.; Golden, D. M.; Kurylo, M. J.; Moortgat, G. K.; Wine, P. H.; Ravishankara, A. R.; Kolb, C. E.; Molina, M. J.; Finlayson-Pitts, B. J.; Huie, R. E.*, et al.*, Chemical Kinetics and Photochemical Data for Use in Atmospheric Studies : Evaluation Number 15. Pasadena, CA : Jet Propulsion Laboratory, California Institute of Technology: 2006.
59. Sangwan, M.; Krasnoperov, L. N. Kinetics of the Gas Phase Reaction $CH_3 + HO_2$. *J. Phys. Chem. A* **2013,** *117*, 2916-2923.
60. Sangwan, M.; Yan, C.; Chesnokov, E. N.; Krasnoperov, L. N. Reaction $CH_3 + CH_3 \rightarrow C_2H_6$ Studied over the 292 -714 K and 1 – 100 bar Pressure Ranges. *J. Phys.Chem.A* **2015,** *119*, 7847–7857.
61. Manion, J. A.; Huie, R. E.; Levin, R. D.; Jr., D. R. B.; Orkin, V. L.; Tsang, W.; McGivern, W. S.; Hudgens, J. W.; Knyazev, V. D.; Atkinson, D. B.*, et al.*, NIST Chemical Kinetics Database, NIST Standard Reference Database 17, Version 7.0 (Web Version), Release 1.4.3, Data version 2008.12, National Institute of Standards and Technology, Gaithersburg, Maryland, 20899-8320. Web address: http://kinetics.nist.gov/. 2008.
62. Burkholder, J. B.; Sander, S. P.; Abbatt, J.; Barker, J. R.; Huie, R. E.; Kolb, C. E.; Kurylo, M. J.; Orkin, V. L.; Wilmouth, D. M.; Wine, P. H. Chemical Kinetics and Photochemical Data for Use in Atmospheric Studies, Evaluation No. 18, JPL Publication 15-10, Jet Propulsion Laboratory. http://jpldataeval.jpl.nasa.gov (accessed September 2019).
63. Ravishankara, A. R.; Wine, P. H.; Nicovich, J. M. Pulsed Laser Photolysis Study of the Reaction between Atomic Oxygen (^{3}P) and Hydroperoxo Radical. *J. Chem. Phys.* **1983,** *78*, 6629-6639.
64. Morin, J.; Romanias, M. N.; Bedjanian, Y. Experimental Study of the Reactions of OH Radicals with Propane, n-Pentane, and n-Heptane over a Wide Temperature Range. *Int. J. Chem. Kinet.* **2015,** *47*, 629-637.
65. Bedjanian, Y.; Le Bras, G.; Poulet, G. Kinetic Study of the Reactions of Br_2 with OH and OD. *Int. J. Chem. Kinet.* **1999,** *31*, 698-704.
66. Su, M. C.; Kumaran, S. S.; Lim, K. P.; Michael, J. V.; Wagner, A. F.; Harding, L. B.; Fang, D. C. Rate Constants, $1100 \leq T \leq 2000$ K, for $H + NO_2 \rightarrow OH + NO$ Using Two Shock Tube Techniques: Comparison of Theory to Experiment. *J. Phys. Chem. A* **2002,** *106*, 8261-8270.
67. Bedjanian, Y. Temperature-Dependent Rate Constant for the Reaction of Hydroxyl Radical with 3-Hydroxy-3-Methyl-2-Butanone. *J. Phys. Chem. A* **2019,** *123*, 10446-10453.
68. SCIENTIST *Micromath Scientific Software. Saint Louis, MO.*
69. Bedjanian, Y.; Kalyan, C. Rate Constants of the Reactions of O(^{3}P) Atoms with Br_2 and NO_2 over the Temperature Range 220-950 K. *Int. J. Chem. Kinet.* **2019,** *51*, 476-483.
70. Dulitz, K.; Amedro, D.; Dillon, T. J.; Pozzer, A.; Crowley, J. N. Temperature-(208–318 K) and Pressure-(18–696 Torr) Dependent Rate Coefficients for the Reaction between OH and HNO_3. *Atmos. Chem. Phys.* **2018,** *18*, 2381-2394.

71. Bedjanian;, Y.; Ravishankara, A. R. Low Pressure Reaction Kinetics of OH+HNO_3 in an Extended Temperature Range, *The Eleventh International Conference on Chemical Kinetics,* Orléans, France, 2019, https://icck2019.sciencesconf.org/data/pages/ICCK_Proc_final.pdf.
72. Amedro, D.; Bunkan, A. J. C.; Berasategui, M.; Crowley, J. N. Kinetics of the OH + NO_2 Reaction: Rate Coefficients (217–333 K, 16–1200 mbar) and Fall-off Parameters for N_2 and O_2 Bath Gases. *Atmos. Chem. Phys.* **2019,** *19*, 10643-10657.
73. Gericke, K. H.; Comes, F. J. Energy Partitioning in the Reaction Atomic Oxygen (^1D) + Water → Hydroxyl Radical + Hydroxyl Radical. *Chem. Phys. Lett.* **1980,** *74*, 63-66.
74. Nguyen, T. L.; Stanton, J. F. Ab Initio Thermal Rate Calculations of HO + HO ––> O(^3P) + H_2O Reaction and Isotopologues. *J. Phys. Chem. A* **2013,** *117*, 2678-2686.
75. Russell, J. J.; Seetula, J. A.; Gutman, D. Kinetics and Thermochemistry of CH_3, C_2H_5, and i-C_3H_7. Study of the equilibrium R + HBr = R-H + Br. *J. Am. Chem. Soc.* **1988,** *110*, 3092-3099.
76. Seakins, P. W.; Pilling, M. J.; Niiranen, J. T.; Gutman, D.; Krasnoperov, L. N. Kinetics and Thermochemistry of R + HBr = RH + Br Reactions: Determinations of the Heat of Formation of C_2H_5, i-C_3H_7, sec-C_4H_9, and t-C_4H_9. *J. Phys. Chem.* **1992,** *96*, 9847-9855.
77. Kalinovski, I. J.; Gutman, D.; Krasnoperov, L. N.; Goumri, A.; Yuan, W.-J.; Marshall, P. Kinetics and Thermochemistry of the Reaction $Si(CH_3)_3$ + HBr = $Si(CH_3)_3H$ + Br: Determination of the $(CH_3)_3$Si-H Bond Energy. *J. Phys. Chem.* **1994,** *98*, 9551-9557.
78. Krasnoperov, L. N.; Peng, J.; Marshall, P. Modified Transition State Theory and Negative Apparent Activation Energies of Simple Metathesis Reactions: Application to the Reaction CH_3 + HBr → CH_4 + Br. *J. Phys. Chem. A* **2005,** *110*, 3110-3120.
79. Gao, Y.; Alecu, I. M.; Hsieh, P.-C.; Morgan, B. P.; Marshall, P.; Krasnoperov, L. N. Thermochemistry Is Not a Lower Bound to the Activation Energy of Endothermic Reactions: A Kinetic Study of the Gas-Phase Reaction of Atomic Chlorine with Ammonia. *J. Phys. Chem. A* **2006,** *110*, 6844-6850.

TOC Graphic